Mie Resonance Based Dielectric Nano Cylinders

A Dissertation submitted towards the partial fulfilment of
the requirement for the award of degree of

Master of Technology in
Microwave and Optical Communication Engineering

Submitted by
PARAS KUMAR
2K14/MOC/10

Under the supervision of
Dr. Yogita Kalra
Assistant Professor

Department of Applied Physics and Department of
Electronics & Communication Engineering

Delhi Technological University
(Formerly Delhi College of Engineering)

JUNE 2016

DELHI TECHNOLOGICAL UNIVERSITY

Established by Govt. of Delhi vide Act 6 of 2009
(*Formerly Delhi College of Engineering)*
SHAHBAD DAULATPUR, BAWANA ROAD, DELHI-110042

CERTFICATE

This is to certify that the work which is being presented in the dissertation entitled

"Mie resonance based dielectric nano cylinders" is the authentic work of Paras Kumar under my guidance and supervision in the partial fulfillment of requirement towards the degree of Master of Technology in Microwave and Optical Communication Engineering jointly run by Department of Applied Physics and Department of Electronics and Communication in Delhi Technological University during the 2014-16.

As per the candidate declaration this work has not been submitted elsewhere for the award of any other degree.

Dr. Yogita Kalra (Supervisor)
Assistant Professor
Department of Applied Physics
DTU

Prof. Rajesh Rohilla
Professor
Head of Department
Electronics and Communication
DTU

Prof. S.C. Sharma
Professor
Head of Department
Applied Physics
DTU

DECLARATION

I hereby declare that all the information in this document has been obtained and presented in accordance with academic rules and ethical conduct. This report is my own, unaided work. I have fully cited and referenced all material and results that are not original to this work. It is being submitted for the degree of Master of Technology in Microwave and Optical Communication Engineering at Delhi Technological University. It has not been submitted for any degree or examination in any other university.

Paras Kumar
M. Tech, MOCE
2K14/MOC/10

Abstract

Based on Maxwell's equations and Mie theory, strong subwavelength artificial magnetic and electric dipole resonances can be excited within dielectric resonators and their resonant frequencies can be tailored simply by scaling the size of the dielectric resonators. This work is based on Mie resonance in dielectric nano cylinders. To generalize the result, different aspect ratio (height to radius ratio) of cylinder have been simulated. It is a well-known fact that first and second resonance of dielectric particles correspond to magnetic and electric dipole terms. Interference of optically induced magnetic and electric modes in high refractive index dielectric nano particles offers unique possibility for tailoring directional scattering and engineering the flow of light. The optical properties such as reflection coefficient, scattering cross section, relative permeability and relative permittivity of silicon nano cylinders are calculated. The optical parameters mentioned above are observed by changing the aspect ratio. The wavelength corresponding to maximum scattering extinction shifts to longer wavelengths as the height of the nanoparticle is increased. The red shift is accompanied by an increase in the scattering cross section peak intensity. The impact of higher order multipoles for large nanoparticles makes the spectra complex observed. The peak position for the nano cylinders with different aspect ratio matches the resonant wavelength. This model can be used to interpret optical properties for a cylinder when its height is increased. The scattering cross section peaks are mainly because of the magnetic and electric dipole contributions. Resonance positions are conformed from the transmission coefficient graph. From the relative permittivity and permeability calculations using the s-parameter retrieval technique, the resonance positions are reconfirmed. The demonstrated properties of silicon nano cylinders could be used for the realization of dielectric metasurfaces with different functional optical properties, in the field of nanoantennas, nanolasers, photovoltaics and even in biomedicine.

ACKNOWLEDGEMENT

The thesis work is a result of hard work and contribution of many well-wishers, whose support and guidance has resulted in timely completion of project.

I would like to express my deepest gratitude to my supervisor **Dr. Yogita Kalra**, Asst Professor, Department of Applied Physics, who accepted request of being my guide and for her invaluable support, quality guidance, priceless knowledge and constant motivation throughout the period of the project that has helped in timely completion and submission of this thesis.

I am deeply grateful to **Prof. S.C. Sharma**, H.O.D (Dept of A.P.), **Prof. Rajesh Rohilla**, H.O.D (Dept. of ECE), **Prof R.K. Sinha**, **Prof. Rajiv Kapoor**, **Dr. Ajeet Kumar** for their support, and also for providing us with all the facilities to carry out quality project work.

I would like to thank Mr. Nishant Shankhawar, research scholar for his valuable time and interest in the project. His knowledge, advice and time bound solutions for the queries raised during the course of the project have helped me in timely completion of the project work.

I also wish to express my heart full thanks to the classmates as well as staff at Department of Applied Physics and Department of Electronics and Communication of Delhi Technological University for their goodwill and support that helped me a lot, in successful completion of this project.

Finally, I want to thank my parents, for inculcating good ethos, as a result of which I am able to do my post-graduation from such an esteemed institution.

Paras Kumar
M.Tech.
MOCE
2K14/MOC/10

TABLE OF CONTENTS

LIST OF FIGURES

Chapter 1

Introduction

The capability to control and engineer electromagnetic scattering of waves by subwavelength nano designs is of great importance in some of the upcoming fields of nanophotonics. It has various applications in the field of nanoantennas, photovoltaics, biomedicine and to the extent of nanolasers[1-7]. Metallic nanoparticles do promise in capturing, focusing and manipulating light at nanoscale dimensions [1,8,9]. As seen through multiple applications in our daily life, it creates the way for miniature plasmonic devices and nanophotonic circuits by overcoming the bottleneck of the traditional limit of light [9]. But, metallic building blocks for negative permittivity and permeability is not preferred because they suffer from high energy dissipation, conductive losses and anisotropic responses.

This is where dielectric metamaterials come into picture. Metamaterials are artificial structures composed of microscopic elements whose aggregate behavior results in unusual macroscopic optical properties and applications [10-12]. To scale down metamaterials to optical frequencies is still a challenging issue. Such an accomplishment would accelerate the development of novel and sophisticated optical technologies in many areas, such as solar power, telecommunications and even life sciences. Recent works [13-18] have proposed to use high permittivity dielectric objects rather than metallic ones to surpass the losses and saturation effects which are built-in to the metal in optical range [19]. This approach depends on the resonant modes which are supported by that dielectric object. High permittivity dielectric objects are used as constitutive elements of new metamaterials and antennas based on dielectric resonators [21, 22, 23]. But magneto dielectric properties are usually accompanied with low loss and large dielectric constants accessible at microwave and terahertz frequencies. This still remains a major challenge in the infrared and visible frequency ranges. But, it has been shown that silicon rod arrays could show a true metamaterial left hand dispersion branch in the visible to mid infrared even with the mild value of refractive index (m~3.5).

Motivated by the above mentioned results, the magneto dielectric properties of lossless dielectric cylindrical particles with moderate permittivity materials in IR region are examined. Although the analysis of scattering resonances of homogenous spheres have been analyzed in the past [19, 23, 24] the main focus is on the first dipolar resonance in non-absorbing dielectric cylinder. Later the same principle is applied to cylinder and the behavioral changes are observed when the aspect ratio is changed to make it disc and rod respectively. Interestingly, it has been observed that dielectric rods in p-polarized light (electric field perpendicular to rod axis) could exhibit both electric and magnetic resonances, and so constitute a left handed medium with simultaneously negative permittivity and permeability. These dipolar resonances could be explained with the help of strong charge displacement and displacement currents, but to our knowledge, no theory has been proposed. In this work, scattering of an incident electromagnetic wave by a cylindrical particle whose height could be varied (disk to finite rod) has been analyzed. The solutions provide details of scattering cross section, electric and magnetic resonances.

1.1 Thesis Objective

The main objectives of the thesis are given as follows:

- To study of the Maxwell's equations and basic Mie theory related to the scattering properties of all dielectric nanoparticles.
- To study and understand the theory behind the resonance mechanism of the dielectric nanoparticles at infrared frequencies.
- To study the optical properties like scattering cross section, transmission coefficient, relative permittivity and relative permeability of nano cylinders by varying the aspect ratio.

1.2 Thesis Organization

Chapter 2

This chapter is a brief introduction to scattering theory and Mie theory in general. Light scattering by sphere is discussed and vector wave equation solutions are deduced. Equations

for Mie coefficients and scattered fields have been derived. Different cross section calculations are also discussed.

Chapter 3

Simulation software used in this project work is introduced in this chapter. COMSOL Multiphysics and Matlab are discussed briefly.

Chapter 4

Mie resonance and its mechanism are introduced in this chapter. Procedure to calculate the scattering cross section of sphere and of cylinder using COMSOL Multiphysics is discussed in brief. Scattering cross section obtained for a dielectric sphere is plotted against wavelength. Retrieval technique for relative permittivity and relative permeability from s-parameters is also discussed.

Chapter 5

This chapter contains the simulated results from the port analysis for nano cylinder with varying aspect ratio achieved with the help of COMSOL Multiphysics and the graphs of electric and magnetic field lines are plotted to discuss the resonance features. Finally, according to the values obtained for transmission coefficients, relative permeability and relative permittivity, the type of resonance is discussed.

Chapter 6

The thesis is concluded in this chapter. Various conclusions have been summarized and future scope has been discussed.

Chapter 2

Theoretical Background

Scattering of light is the redirection of light when an electromagnetic wave confronts an obstacle, in our case the scattering particle. When the electromagnetic wave interacts with the discrete scattering particle, the electron orbits within the particle's composing molecules , are agitated periodically with similar frequency (ϑ_0) as of the incident electric field. Due to perturbation or oscillation of the electron cloud, the charge within the molecule is separated, which we call induced dipole moment. This oscillating induced dipole moment results in the scattering of light. Elastic scattering of light refers to scattered light which is emitted at the identical frequency (ϑ_0) of the incident electromagnetic wave. In other words, light scattering is a complex interaction between scattering object and the incident electromagnetic wave.

2.1 Introduction

There are two theoretical frameworks for defining light scattering theory. One theory is Rayleigh scattering and other Mie scattering. Rayleigh scattering is named after Lord Rayleigh, that was originally formulated and applicable to small, dielectric, non-absorbing spherical particles. On the other hand, Mie theory is named after Gustav Mie that includes the general spherical solution that may be absorbing or non-absorbing. Mie theory is the basic tool for spherical particles. But Rayleigh scattering theory is generally preferred if it is applicable because Mie scattering formulation is complex in nature. Rayleigh scattering takes place when it meets the condition that $\alpha \ll 1$ and $|m|\alpha << 1$, where 'α' is the dimensionless size parameter given by

$$\boldsymbol{\alpha} = \frac{2\pi a}{\lambda} \tag{2.1}$$

Where '*a'* is the radius of the spherical particle and 'λ' is the relative scattering wavelength defined as

$$\lambda = \frac{\lambda_0}{m_0} \tag{2.2}$$

Where 'λ_0' represents the incident wavelength with respect to vacuum, and m_0 is the refractive index of the medium. Refractive index of the scattering particle is denoted by *m* which is generally complex in nature and defined as

$$m = n - ik \tag{2.3}$$

Here *n* refers to refraction of light which equals to the speed of light in vacuum divided by the speed of light in the medium and the complex term is related to absorption. Generally, the absorption coefficient of the material is related to the complex part of the refractive index as

$$absorption\ coefficient = \frac{4\pi\kappa}{\lambda} \tag{2.4}$$

The value of 'κ' is a plays a very important role in defining the type of material. Its value is never exactly zero for any material, but when its value approaches zero, those materials are termed as dielectrics.

2.2 The light scattering problem

Electromagnetic field is scattered in all directions when incident on an object. So, depending on the optical and geometrical properties of the object and the surroundings, incident and scattered fields will have unlike characteristics. Hence, from the scattered field characteristics, some idea about the object can be formulated. There are two different approaches to solve the light scattering problem. First one is to get the scattered radiation using the properties of the object and second approach determines the characteristics of object using the scattered field properties. The second approach is referred as the inverse problem approach [23]. For this thesis, Mie theory with the simplest geometry of sphere has been studied and later on, these results and conclusions are directly used for cylinder.

2.3 Light scattering by sphere

Mie theory gives the solution for the electromagnetic scattering by a spherical particle. It is assumed that this spherical particle is present in a linear, homogenous and isotropic medium illuminated by a plane wave. The mathematics for Mie theory is straightforward but the

underlying physics of the interaction of the sphere with the electromagnetic wave is very complicated.

2.4 Vector wave equation solutions

In a linear, homogenous and isotropic medium, a time harmonic electromagnetic field $(\vec{E}, \vec{H})$ satisfies the wave equation

$$\nabla^2\vec{E} + \mathrm{k}^2\vec{E} = 0 \tag{2.5}$$

$$\nabla^2\vec{H} + \mathrm{k}^2\vec{H} = 0 \tag{2.6}$$

where $\mathrm{k}^2 = \omega^2\varepsilon\mu$, ω is the incident field frequency, ε is the electric permittivity and μ is the magnetic permeability. Electric and magnetic fields are divergence free as the charge density is zero, i.e.

$$\nabla.\vec{E} = 0 \tag{2.7}$$

$$\nabla.\vec{H} = 0 \tag{2.8}$$

In addition, considering the time harmonicity of the fields, $\vec{E}$ and $\vec{H}$ are not independent, i.e.

$$\nabla \times \vec{E} = i\omega\mu H \tag{2.9}$$

$$\nabla \times \vec{H} = -i\omega\varepsilon\vec{E} \tag{2.10}$$

To make the solution of the wave equation comparatively easy, an intermediate vector function $\vec{M}$ is introduced such that

$$\vec{M} = \nabla \times (\vec{c}\psi) \tag{2.11}$$

Where $\vec{c}$ is a constant vector and ψ being a scalar function.

It is known that divergence of curl of any vector function is equal to zero,

$$\nabla.\vec{M} = 0 \tag{2.12}$$

Using vector identities and applying operator $\nabla^2 + \mathrm{k}^2$ we obtain the following results

$$\nabla^2\vec{M} + \mathrm{k}^2\vec{M} = \nabla \times [\vec{c}(\nabla^2\psi + \mathrm{k}^2\psi)] \tag{2.13}$$

Comparing equation 2.5, 2.6 and 2.13, it is observed that $\vec{M}$ satisfies the wave equation, if ψ is a solution to the scalar equation

$$\nabla^2\psi + \mathrm{k}^2\psi = 0 \tag{2.14}$$

or, $\vec{M}$ can also be written as

$$\vec{M} = -\vec{c} \times \nabla\psi \tag{2.15}$$

The above equation shows that $\vec{M}$ is perpendicular to $\vec{c}$. Here the intermediate function $\vec{M}$ represents the electric or magnetic field. To denote the other field another divergence free vector function that satisfies the wave equation is assumed such that

$$\vec{N} = \frac{\nabla \times \vec{M}}{k} \tag{2.16}$$

or equivalently

$$\nabla \times \vec{N} = k\vec{M} \tag{2.17}$$

In general, $\vec{M}$ and $\vec{N}$ are called Vector Spherical Harmonics (VSHs), which satisfy all criteria for an electromagnetic field in vacuum:

- Both satisfy wave equation 2.5 and 2.6
- Both are divergence free
- The curl of $\vec{M}$ is proportional to $\vec{N}$
- The curl of $\vec{N}$ is proportional to $\vec{M}$

But the above criteria is true only when ψ is a solution of equation 2.14. Therefore, rather than solving the vector wave equation, which is complex task, the scalar wave equation is solved where ψ is called the generating function and $\vec{c}$ the guiding or pilot vector.

As a spherical particle is considered, spherical coordinates would be suitable to use. The choice of guiding vector is arbitrary. For our convenience, an easy alternative, $\vec{c} = \vec{r}$, is chosen where $\vec{r}$ is the vector position.

The scalar wave equation in spherical coordinates can be written as:

$$\frac{1}{r^2}\frac{\partial}{\partial r}\left(r^2\frac{\partial\psi}{\partial r}\right) + \frac{1}{r^2\sin\theta}\frac{\partial}{\partial\theta}\left(\sin\theta\frac{\partial\psi}{\partial\theta}\right) + \frac{1}{r^2\sin\theta}\left(\frac{\partial^2\psi}{\partial\phi^2}\right) + k^2\psi = 0 \tag{2.18}$$

Assuming a particular form of scalar function ψ as

$$\psi(r,\theta,\phi) = R(r)\Theta(\theta)\Phi(\phi) \tag{2.19}$$

Using separation of variables technique we solve the equation 2.19, one for each coordinate. The solution of these equations must be single valued and must satisfy the conditions of linear independence. Therefore the complete solution of the scalar wave equation is given by

$$\psi_{emn}(r,\theta,\phi) = \cos m\phi P_n^m(\cos\theta) z_n(kr) \tag{2.20}$$

$$\psi_{omn}(r,\theta,\phi) = \sin m\phi P_n^m(\cos\theta) z_n(kr) \tag{2.21}$$

where, *e* and *o* refers to even and odd respectively. P_n^m is the associated Legendre functions of the first kind of degree n and order m and z_n refers to any of the four spherical Bessel functions: j_n, y_n, $h_n^{(1)}$, $h_n^{(2)}$. In figure 2.1, $j_n(x)$ and $y_n(x)$, n = 0,1,2,3,4 are shown for real values of x. $h_n^{(1)}$and $h_n^{(2)}$ are called as spherical Hankel functions which can be expressed as

$$h_n^{(1)}(\rho) = j_n(\rho) + iy_n(\rho) \tag{2.22}$$

$$h_n^{(2)}(\rho) = j_n(\rho) - iy_n(\rho) \tag{2.23}$$

Now, VSHs can be expressed as,

$$\vec{M}_{emn} = \nabla \times (\vec{r}\psi_{emn}) \qquad \vec{M}_{omn} = \nabla \times (\vec{r}\psi_{omn}) \tag{2.24}$$

$$\vec{N}_{emn} = \frac{\nabla \times (\vec{r}\psi_{emn})}{k} \qquad \vec{N}_{mn} = \frac{\nabla \times (\vec{r}\psi_{omn})}{k} \tag{2.25}$$

So, the conclusion from the above theory is that solution of the wave equation can be understood as the series of vector harmonics given by equations 2.24 and 2.25.

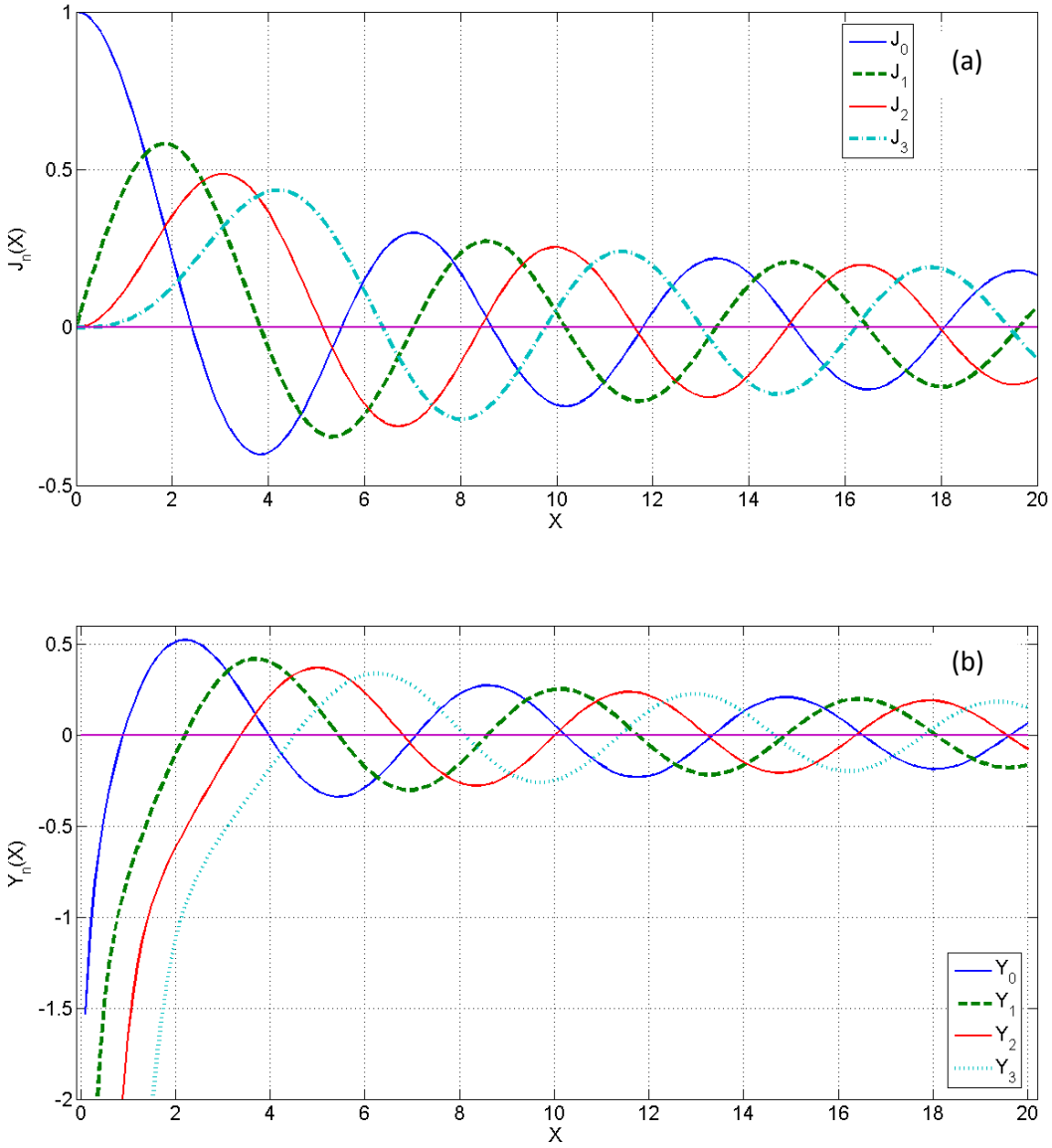

Figure 2.1: Spherical Bessel function of the first (a) and second (b) kind

2.5 Scattered fields and incident fields

The incident wave which is propagating in z direction and is linearly polarized parallel to x-axis can be written as:

$$\vec{E}_i = E_0 e^{ikrcos\theta}\widehat{e_x} \tag{2.26}$$

where E_0 is the electric field amplitude, k is the wave number and $\widehat{e_x}$ is the unit vector in the polarization direction and can be written as:

$$\widehat{e_x} = \sin\theta\cos\phi\,\widehat{e_r} + \cos\theta\cos\phi\,\widehat{e_\theta} - \sin\theta\,\widehat{e_\phi} \tag{2.27}$$

The magnetic field can be obtained using equation 2.26, using curl of electric field. With the help of expanded infinite series of Vector Spherical coordinates, incident field can be written as:

$$\vec{E}_i = \sum_{m=0}^{\infty}\sum_{n=m}^{\infty}(B_{emn}\vec{M}_{emn} + B_{omn}\vec{M}_{omn} + + A_{emn}vec\vec{N}_{emn} + A_{omn}\vec{N}_{omn}) \tag{2.28}$$

where, B_{emn}, B_{omn}, A_{emn}, A_{omn} are the expansion coefficients. Using the orthogonality of the vector harmonics and assuming that the incident field is infinite at the origin, incident electric field can be written as

$$\vec{E}_i = \sum_{n=1}^{\infty}(B_{o1n}\vec{M}_{o1n}^{(1)} + A_{e1n}\vec{N}_{e1n}^{(1)} \tag{2.29}$$

After some manipulations, the final form of the expansion coefficients are

$$B_{o1n} = i^n E_0 \frac{2n+1}{n(n+1)} \tag{2.30}$$

$$A_{e1n} = -i^n E_0 i^n \frac{2n+1}{n(n+1)} \tag{2.31}$$

Substituting equations (2.30) and (2.31) in equation (2.29), the incident electric field becomes

$$\vec{E}_i = E_0 \sum_{n=1}^{\infty} i^n \frac{2n+1}{n(n+1)}(\vec{M}_{o1n}^{(1)} - \vec{N}_{e1n}^{(1)}) \tag{2.32}$$

and the incident magnetic field is given by

$$\vec{H}_i = \frac{-k}{\omega\mu} E_0 \sum_{n=1}^{\infty} i^n \frac{2n+1}{n(n+1)} (\vec{M}_{o1n}^{(1)} + \vec{N}_{e1n}^{(1)}) \tag{2.33}$$

To make the equation look more simpler, $E_n = E_0 i^n \frac{2n+1}{n(n+1)}$ is used.

By applying boundary conditions between sphere and the surrounding medium, scattered field ($\vec{E}_s, \vec{H}_s$) can be easily calculated.

$$(\vec{E}_i + \vec{E}_s - \vec{E}_l) \times \hat{e_r} = (\vec{H}_i + \vec{H}_s - \vec{H}_l) \times \hat{e_r} \tag{2.34}$$

$$\vec{E}_s = \sum_{n=1}^{\infty} E_n (i a_n \vec{N}_{e1n}^{(3)} - b_n \vec{M}_{o1n}^{(3)}) \tag{2.35}$$

$$\vec{H}_s = \sum_{n=1}^{\infty} E_n (i b_n \vec{N}_{o1n}^{(3)} - a_n \vec{M}_{e1n}^{(3)}) \tag{2.36}$$

where the superscript (3) refers to the radial dependence of the generating function, ψ, which is given by spherical Hankel function $h_n^{(1)}$. The coefficients a_n and b_n are called Mie coefficients of the scattered field. Again applying boundary conditions (equation 2.34) at the surface of the sphere, we obtain four equations. These equations can be used analytically to deduce the expressions for Mie coefficients.

$$a_n = \frac{\mu m^2 j_n(mx)[x j_n(x)]' - \mu_l j_n(x)[mx j_n(mx)]'}{\mu m^2 j_n(mx)[x h_n^{(1)}(x)]' - \mu_l h_n^{(1)}(x)[mx j_n(mx)]'} \tag{2.37}$$

$$b_n = \frac{\mu_l j_n(mx)[x j_n(x)]' - \mu j_n(x)[mx j_n(mx)]'}{\mu_l j_n(mx)[x h_n^{(1)}(x)]' - \mu h_n^{(1)}(x)[mx j_n(mx)]'} \tag{2.38}$$

Where μ_l and μ are the magnetic permeabilities of the sphere of the surrounding medium. Again, *m* is the relative refractive index between the medium and the sphere and *x* is the size parameter, which can be defined as

$$x = kR = \frac{2\pi R n}{\lambda} \tag{2.39}$$

$$m = \frac{n_l}{n} \tag{2.40}$$

Where, R is the radius of the sphere, λ is the incident wavelength and n_l and n is the refractive index of the sphere and the medium surrounding it, respectively. Using the Ricatti-Bessel functions, the Mie coefficients for the scattered field can be more simplified.

$$\psi_n(\rho) = \rho j_n(\rho) \tag{2.41}$$

$$\xi_n(\rho) = \rho h_n^{(1)}(\rho) \tag{2.42}$$

For the most general case we assume both the permeabilities of medium and the particle are equal to one, and then Mie coefficients can be expressed as

$$a_n = \frac{m\psi_n(mx)\psi_n'(x) - \psi_n(x)\psi_n'(mx)}{m\psi_n(mx)\xi_n'(x) - \xi_n(x)\psi_n'(mx)} \tag{2.43}$$

$$b_n = \frac{\psi_n(mx)\psi_n'(x) - m\psi_n(x)\psi_n'(mx)}{\psi_n(mx)\xi_n'(x) - m\xi_n(x)\psi_n'(mx)} \tag{2.44}$$

For the most general case, equation 2.43 and 2.44 is considered when the particle presents electric and magnetic properties. Electric permittivity and magnetic permeability of the particle can take values other than one. Choosing the magnetic permeability of the medium as one, the Mie coefficients can be expressed as

$$a_n = \frac{\tilde{m}\psi_n(mx)\psi_n'(x) - \psi_n(x)\psi_n'(mx)}{\tilde{m}\psi_n(mx)\xi_n'(x) - \xi_n(x)\psi_n'(mx)} \tag{2.45}$$

$$b_n = \frac{\psi_n(mx)\psi_n'(x) - \tilde{m}\psi_n(x)\psi_n'(mx)}{\psi_n(mx)\xi_n'(x) - \tilde{m}\xi_n(x)\psi_n'(mx)} \tag{2.46}$$

where, $\tilde{m} = \frac{m}{\mu_l}$ and $\mu = 1$.

2.6 Different Cross Section calculations

From the scattered fields, we can obtain important physical quantities. One of them is cross section. Cross section is defined as the net rate at which the electromagnetic energy (W) crosses the surface of an imaginary sphere of radius $r \geq R$ centered by the particle divided by the irradiance (I_i) [23]. The absorption (σ_{abs}) or scattering cross section (σ_{sc}) is defined to measure the rate of electromagnetic energy that is absorbed (W_{abs}) or scattered (W_{sca}) by the diffuser.

$$\sigma_{abs} = \frac{W_{abs}}{I_i} \tag{2.47}$$

$$\sigma_{sc} = \frac{W_{sca}}{I_i} \tag{2.48}$$

The sum of absorption and scattering cross section gives us the extinction coefficient which tells about the amount of energy removed from the incident field due to scattering and/or absorption generated by the particle [23].

$$\sigma_{ext} = \sigma_{sc} + \sigma_{abs} \tag{2.49}$$

In terms of Mie coefficients, the above mentioned parameters can be expressed as follows

$$\sigma_{sc} = \frac{W_{sca}}{I_i} = \frac{2\pi}{k^2}\sum_{n=1}^{\infty}(2n+1)(|a_n|^2 + |b_n|^2) \tag{2.50}$$

$$\sigma_{ext} = \frac{W_{ext}}{I_i} = \frac{2\pi}{k^2}\sum_{n=1}^{\infty}(2n+1)Re(a_n + b_n) \tag{2.51}$$

$$C_{abs} = C_{ext} - C_{sca} \tag{2.52}$$

To obtain the scattering, extinction and absorption efficiencies, these cross sections are divided by the geometrical cross area G of the particle projected onto a plane which is perpendicular to the incident beam. Generalizing for a sphere of radius R, $G = \pi R^2$, these efficiencies would become

$$Q_{sca} = \frac{\sigma_{sc}}{G} = \frac{2}{x^2}\sum_{n=1}^{\infty}(2n+1)(|a_n|^2 + |b_n|^2) \tag{2.53}$$

$$Q_{ext} = \frac{\sigma_{ext}}{G} = \frac{2}{x^2}\sum_{n=1}^{\infty}(2n+1)Re(a_n + b_n) \tag{2.54}$$

$$Q_{abs} = Q_{ext} - Q_{sca} \tag{2.55}$$

Chapter 3

Numerical Simulation methods

In this chapter, a short introduction to the numerical simulation method used is described.

3.1 COMSOL Multiphysics

COMSOL Multiphysics is a comprehensive simulation software environment for a wide array of applications, but structured and user-friendly for all to use. COMSOL is a simulation environment, designed with real-world applications in mind. The point of all simulation of course is to mimic, as closely as possible, effects that are observed in reality. Be they in an engineering or scientific context. To do this, there is the need of multiphysics; that is multiple scientific models that include the things that you are interested in. Some of these are: acoustics, electromagnetics, chemical reactions, mechanics, fluid flow, and heat transfer. Because the real world includes all of these effects, your simulation environment should also. This is what COMSOL seeks to deliver, and we do so in an easy-to-use interface geared toward making scientists and engineers more productive in their day-to-day work.

COMSOL Multiphysics is a finite element analysis, solver and Simulation software / FEA Software package for various physics and engineering applications, especially coupled phenomena, or multiphysics. The package is platform independent. The software has several add on module which can be used to solve and simulate problems in different fields like electromagnetics, mechanics, MEMS, Chemical engineering etc. COMSOL also has MATLAB where the solutions can be exported or imported between these two softwares which help in better and accurate analysis.

Radio frequency (RF) module is used in our work. The RF Module solves problems in the general field of electromagnetic waves, such as RF and microwave applications, optics, and photonics. The underlying equations for electromagnetics are automatically available in all of the physics interfaces, a feature unique to COMSOL Multiphysics. This makes modeling

easily accessible. The module is useful for component design in virtually all areas where we find electromagnetic waves, such as:

- Antennas
- Waveguides and cavity resonators in microwave engineering
- Optical fibers
- Photonic waveguides
- Photonic crystals
- Active devices in photonics

The physics interfaces cover the electromagnetic field simulations and handle time-harmonic, time-dependent, and eigen-frequency/eigen-mode problems either in-plane, axisymmetric, and full 3D electromagnetic wave propagation or full vector mode analysis in 2D and 3D. In addition to the standard post processing features, the module supports direct computation of S-parameters and far-field patterns. This particular feature has reduced the complexity of the problem. Ports could be added with a wave excitation with specified power level and mode type, and add PMLs (perfectly matched layers) to simulate electromagnetic waves that propagate into an unbounded domain. In RF domain, there could be various interfaces such as:

- Electromagnetic waves, Frequency domain
- Electromagnetic waves, Time domain
- Electromagnetic waves, Transient
- Transmission line

Frequency domain interface is used in this work, which gives a variety of analysis either in eigen frequency mode, frequency domain mode or in boundary mode analysis. Frequency domain mode is preferred over time domain because for small step size time domain interface is time consuming. The RF modeling process is simple and has the following steps:

1. We select the appropriate physics interface or predefined multiphysics coupling in the **Model Wizard**.
2. Defining model parameters and variables in the **Definitions** branch.
3. Drawing or importing the model geometry in the **Geometry** branch.

4. Assigning material properties to the geometry in the **Materials** branch.
5. Setting up the model equations and boundary conditions in the physics interfaces branch.
6. Meshing in the **Mesh** branch.
7. Setting up the study and computing the solution in the **Study** branch.
8. And finally analyzing and visualizing the results in the **Results** branch.

Even after a model is defined, it is easy to edit an input data, equations, boundary conditions, geometry, the equations and boundary conditions are still available through associative geometry and mesh settings.

3.2 MATLAB

MATLAB is a high-performance language for technical computing. It integrates computation, visualization, and programming in an easy-to-use environment where problems and solutions are expressed in familiar mathematical notation. Typical uses include:

- Math and computation
- Algorithm development
- Modeling, simulation, and prototyping
- Data analysis, exploration, and visualization
- Scientific and engineering graphics
- Application development, including Graphical User Interface building

MATLAB is an interactive system whose basic data element is an array that does not require dimensioning. This allows us to solve many technical computing problems, especially those with matrix and vector formulations, in a nick of the time it would take to write a program in a scalar non-interactive language such as C or Fortran.

The name MATLAB stands for Matrix laboratory. MATLAB was originally written to provide easy access to matrix software developed by the LINPACK and EISPACK projects, which together represent the state-of-the-art in software for matrix computation. MATLAB has evolved over a period of years with input from many users. In university environments, it is the standard instructional tool for introductory and advanced courses in mathematics,

engineering, and science. In industry, MATLAB is the tool of choice for high-productivity research, development, and analysis.

MATLAB features a family of application-specific solutions called toolboxes. Very important to most users of MATLAB, toolboxes allow us to learn and apply specialized technology. Toolboxes are comprehensive collections of MATLAB functions (M-files) that extend the MATLAB environment to solve particular classes of problems. Areas in which toolboxes are available include signal processing, control systems, neural networks, fuzzy logic, wavelets, simulation, and many others. MATLAB is a high-level matrix/array language with control flow statements, functions, data structures, input/output, and object-oriented programming features. It allows both "programming in the small" to rapidly create quick and dirty throw-away programs, and "programming in the large" to create complete large and complex application programs. In our thesis, we have used MATLAB for various computations and especially for plotting graphs.

Chapter 4

Light scattering resonances by nanoparticles

4.1 Introduction

New technical possibilities like intra chip optical communication or biosensors are possible only due to advancement in nanophotonics. For high optical response and directional control of light scattering small component sizes and novel behaviors are required. This necessity brought technology towards the age of nanometric structures and particles. But the major concern for these systems is their small scattering cross section which affects or alters the propagation of light. It can be overcome if scatterers can sustain resonances. The advantage of sustaining resonances is that it enhances light matter interaction. Due to the ability to confine the electromagnetic waves to regions in space, metallic nano structures are attracting many researchers. They do so with help of localized surface plasmons. These surface plasmons are collective oscillation of the electron plasma at the interface between dielectric and metal, or on the metallic structures surfaces.

Metallic nano structures have various disadvantages owing to which scientists and researchers have now focused their attention towards non-metallic structures like dielectrics. Light resonances also appear in non-metallic structures and have been a great area of interests. We would like to mention the work done by G. Videen and W. Bickel [23]. They have analyzed the Mie resonances for very small dielectric spherical particles. They also have made a complete study of resonances as a function of the refractive index and particle size of the scatterer. Approximations to Mie theory could be used as particles which are considered are much smaller than the incident wavelength. They also proved that the Mie coefficients of order higher than two can be neglected. They also proposed the approximate expressions for the first four Mie coefficients $a_1, a_2, b_1 \; and \; b_2$.

4.2 Mie resonance

It is known that light scattering by a particle depends on the shape, size and optical properties of a scatterer and also on the frequency of the incident wave. Similarly resonances and their

spectral properties depend on optical properties and particle size. To understand more clearly, resonances are excited when the denominator term of the Mie coefficients $a_n \; and \; b_n$(equation 2.43 and 2.44) are zero. The zeros of the denominator appear when

$$m^2 = -\frac{n+1}{n}, \qquad n = 1,2,3 \ldots. \tag{4.1}$$

where 'm' is the refractive index of the particle, relative to the surrounding medium. For non-magnetic particle with an electric permittivity $\varepsilon = \varepsilon' + i\varepsilon''$ immersed in a non-absorbing surrounding medium (ε_m), the resonant behavior for the first order case appears for

$$\varepsilon' = -2\varepsilon_m \qquad and \qquad \varepsilon'' = 0 \tag{4.2}$$

This resonance is known as Frohlich resonance or mode of uniform polarization [23]. Using the generalized expressions for $a_1, a_2, b_1 \; and \; b_2$ analysis of Mie resonance for small but finite size particles can be done. But this work is basically based on the systematic and graphical approach for the scattering Mie resonances for sphere and later it can be extended to nano cylinders. In the case of nano cylinders aspect ratio of the cylinder is varied and then analysis of the results is done. The basic idea is to observe the scattering resonance characteristics while traversing from disk to cylinder and finally to a finite rod.

4.3 Extinction resonances of a dielectric sphere

For this thesis, the main focus is on silicon spheres in the mid infrared region. Even though scattering resonances of uniform sphere have been discussed in the past [19,23,24], the main focus is on the connection of the first magnetic and electric dipolar resonance in the non-absorbing dielectric nano-spheres. From the simulation results, it is observed that submicron silicon spheres with radius $\approx 200\, nm$ can display a strong magnetic response at optical and infrared frequencies. Based on standard Mie theory, if the quadrupolar and higher orders contribution are ignored, then these silicon nano-spheres can be perfectly described by their dipolar electric and magnetic fields.

A dielectric non-absorbing sphere of radius 'a' with refractive index m_p and relative permittivity $\varepsilon_p = m_p^2$ is considered. The medium under consideration is uniform with real relative permittivity ε_h and refractive index $m_h = \sqrt{\varepsilon_h}$. It is assumed that the magnetic

permeability of the sphere and the surrounding, to be 1. Assuming linearly polarized light, the incident wave under plane wave illumination can be described as

$$E = E_0 u_y e^{-ikx} e^{-i\omega t} \tag{4.1}$$

$$B = B_0 u_z e^{-ikx} e^{-i\omega t} \tag{4.2}$$

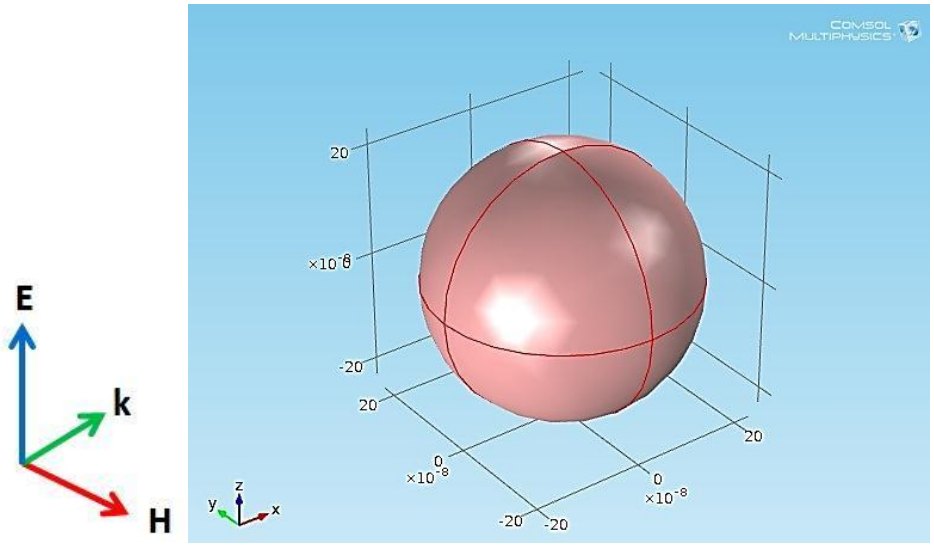

Fig. 4.1 Incident field vector on the nano sphere

where, $k = \frac{m_h \omega}{c} = \frac{m_h 2\pi}{\lambda}$, λ being the wavelength in vacuum and $B_0 = \mu_0 H_0 = -m_h E_0 / c$ (Fig. 1). With the help of Mie expansion, the scattered field can be decomposed into multipole series. This series is characterized by electric and magnetic Mie coefficients $a_n \; and \; b_n$ (equation 2.35 and 2.36) respectively. Here a_1 and b_1 is proportional to the electric and magnetic dipoles, a_2 and b_2 to the quadropoles and so on. In the absence of absorption, the scattering and extinction cross section have the same value.

The scattering cross section of silicon sphere of radius $a = 230\, nm$ in vacuum is plotted in figure 4.2. For large values of particle relative permittivity ($\varepsilon \gg 12$) and in the small particle range (x<<1), sharp resonance peaks are observed in the scattering cross section. At each resonance, the scattering cross section is of the order of λ^2 and scattering cross section is not dependent on refractive index [19]. The first resonant peak corresponds to the magnetic dipole term of coefficient b_1 [19,23]. For wavelengths larger than $\lambda \approx 1200\, nm$, the

scattering cross section is completely governed by the Mie coefficients a_1 and b_1. Or, indirectly it can be said that silicon particles in this regime could be treated as non-Rayleigh dipolar particles [23].

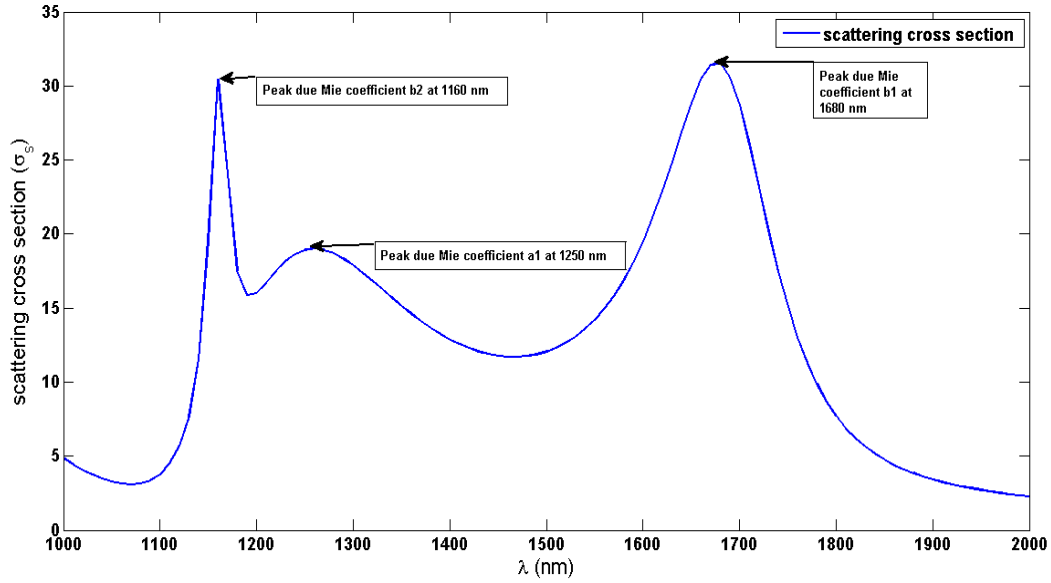

Fig 4.2: Scattering cross section versus wavelength for a 230 nm Si sphere

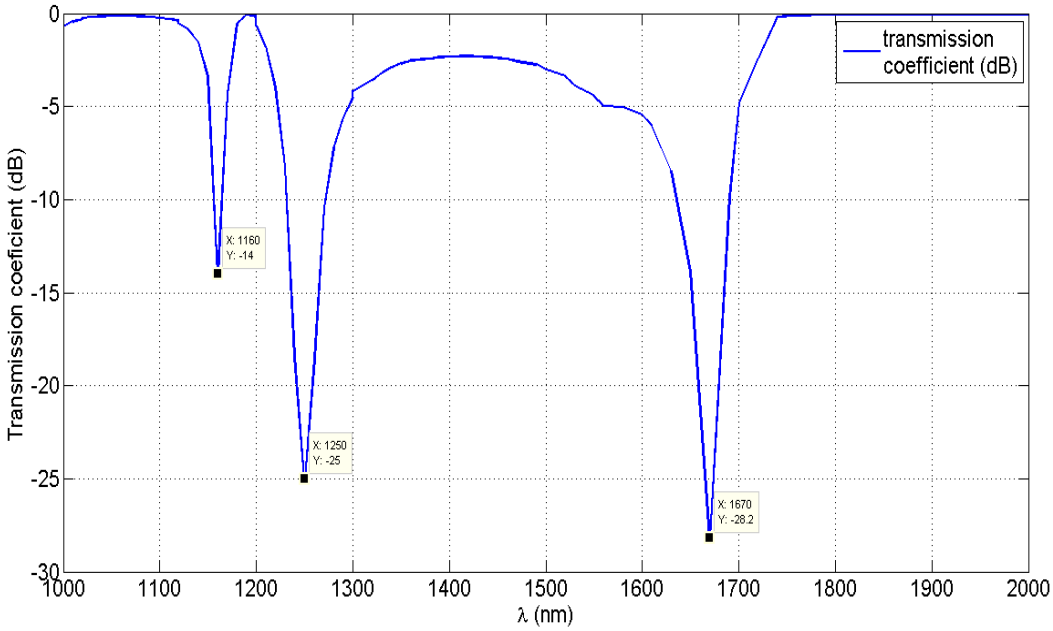

Fig 4.3: Transmission coefficient for a 230 nm nano sphere.

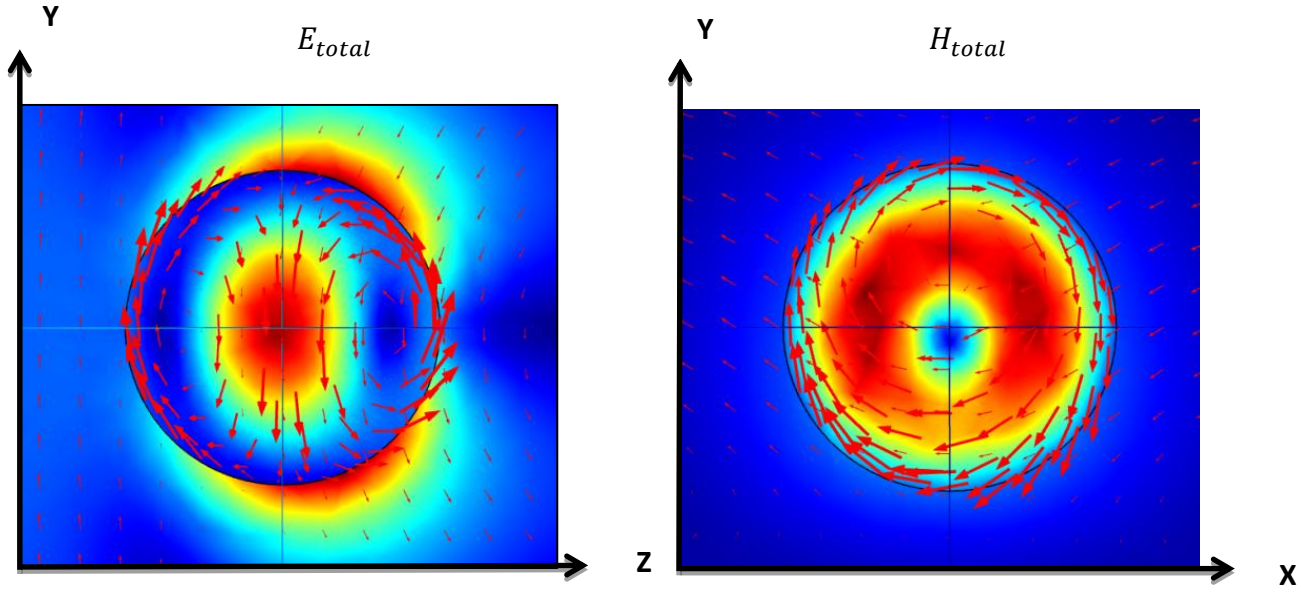

Fig. 4.4: Maps for the square modulus of the total electric and magnetic vectors. The left and right correspond to electric and magnetic peaks of fig. 4.2 at 1250 nm.

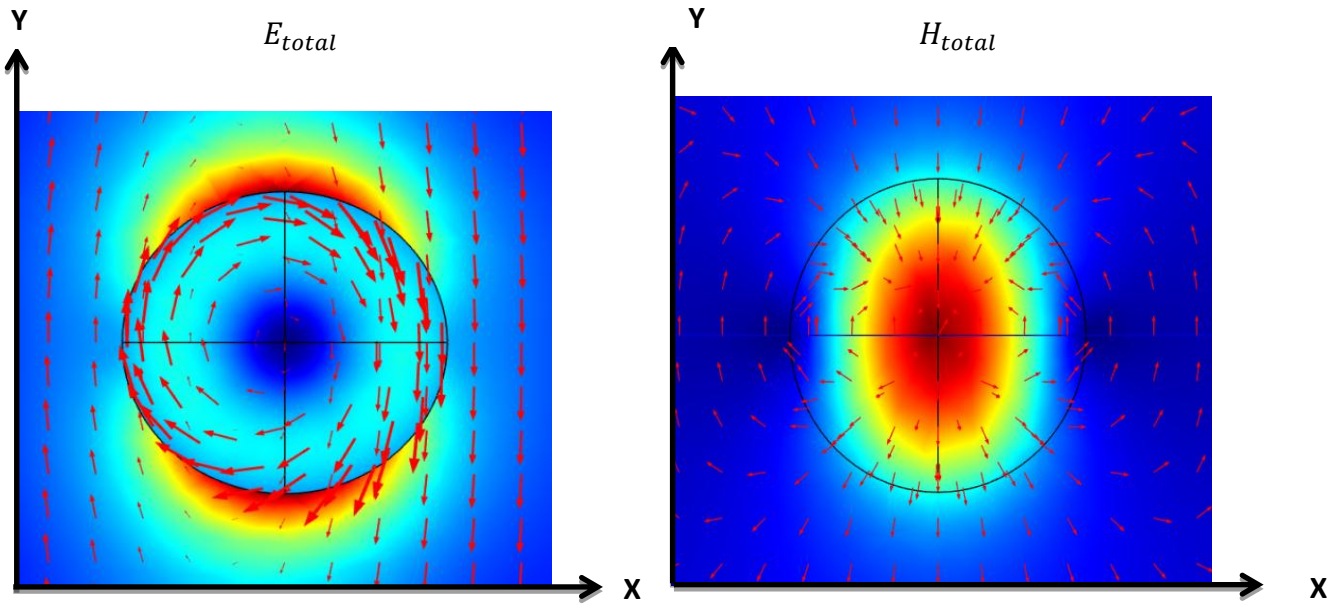

Fig. 4.5: Maps for the square modulus of the total electric and magnetic vectors. The left and right correspond to electric and magnetic peaks of fig. 4.2 at 1680 nm.

Figures 4.4 & 4.5 show that the electric and magnetic field lines inside the sphere. As the magnetic field lines are weak so they are normalized unlike the electric field lines which are plotted proportionately. To understand magnetic resonances (fig. 4.5), field patterns inside

nano sphere at resonance wavelength is studied. One can observe that the near field patterns of dielectric sphere in fig. 4.4 and fig. 4.5 are very similar to those of electric dipole and magnetic dipole oriented along y-direction and z-direction respectively.

4.4 Resonance by cylindrical nanoparticle

From Mie theory, it is clear that the first and the second lowest resonances of dielectric spherical particles correspond to the magnetic and electric terms. There is increase in the quality factors of these Mie resonances and their light scattering efficiency, as the refractive index increases[23]. Due to the above mentioned properties, the dielectric particles having high refractive index are considered as promising building blocks for the concept of metamaterials with negative effective permittivity and permeability. The strong magnetic and electric dipole resonant responses of silicon spherical particles in the infrared region are already discussed. Optical nanoantennas and optical metamaterials are being constructed using the optical properties of spherical particles. It has been theoretically and experimentally shown that the spectral positions of electric and magnetic resonances of silicon nanoparticles can be tuned by altering their shape i.e. by changing their radius [23]. This feature creates a possibility for controlling light scattering characteristics by using silicon nanodisks or nanocylinders with certain size parameters. This is one of the reasons why optical properties of cylindrical shaped dielectric nanoparticles has been deeply studied [25]. Particle size, shape and material are the main parameters which determine the resonant frequency. By making changes in these characteristics, the resonant frequency can be shifted over a wide range of wavelengths. This can make nanoparticles attractive as functional materials for many applications.

For various applications, it is required for the researcher to know the exact wavelengths at which the fundamental resonances occur and these resonances are either due to magnetic diploe or electric dipole. To achieve this goal, the cylindrical nanoparticle whose aspect ratio is varied from disk shape to finite rod is studied in mid infrared region. Here the radius is kept as constant. It is also known that the spectral position of the resonances are dependent on the particle aspect ratio, incident light direction and polarization. In the case of polarization, s-polarized (TE mode) electromagnetic wave is used because it was proposed

to have both electric and magnetic responses [27]. Even for p-polarized (TM mode) wave, it supports both electric and magnetic responses, but in most of the cases only s-polarized wave had been discussed. In s-polarized waves, the electric field (along y–axis) is perpendicular to the rod axis (along z-axis). To get the exact locations of the resonant peaks the scattering cross section is calculated using finite element analysis simulation software COMSOL Multiphysics. From the scattering cross section peaks it is difficult to determine the resonance type, whether it is due to electric dipole or due to magnetic diploe. Using Mie coefficients, and multipole series expansion, one can show the effect of the electric and magnetic dipoles. But this method is tedious and requires complex calculations. So to simplify the approach, COMSOL Multiphysics is used to calculate the scattering cross section. COMSOL allows to directly compute the s-parameters. Using volume average analysis the electric field and electric displacement vector can be calculated. Volume average analysis provides an extra feature to locate the electric resonance point, where the relative permittivity shows a sudden sign change and then behaves normally. The position of the spike tells us about the resonance due to electric dipole and in this region the relative permittivity is negative as in case of left handed metamaterials. After analysis we found that COMSOL uses Maxwell's equation in terms of electric field and relative permittivity. To calculate the relative permeability with this procedure involves complex calculation, which includes solving Maxwell's equation which itself is troublesome and time consuming. Hence an alternative approach for determining the resonance due to magnetic dipole is used. As COMSOL directly calculates the s- parameters, the s-parameters can be directly used to get the relative permeability and relative permittivity using the electromagnetic parametric retrieval technique [28].

4.5 Retrieval of effective permittivity and permeability from S-parameters

The retrieval method used in this work is based on the approach used by Smith et al in [28].The formulation begins by deriving the reflection and transmission coefficients for planar slab geometry. Here it is assumed that the incident wave is TE polarized with a propagation factor of the form, e^{ikz}, i.e., normal incidence. Under this form, the fields in the three regions take the form,

$$E_{1x} = Ae^{ik_1 z} + Be^{-ik_1 z} \tag{4.3}$$

$$H_{1x} = \frac{k_1}{\omega \mu_1}(Ae^{ik_1 z} - Re^{-ik_1 z}) \tag{4.4}$$

$$E_{2x} = Te^{ik_0 z} \tag{4.5}$$

$$H_{2x} = T\frac{k_1}{\omega \mu_1}e^{ik_o z} \tag{4.6}$$

where, it assumed that the material parameters of the incident and transmission region are both given by μ_o and ε_o whereas the slab is characterized by μ_1 and ε_1. Letting the slab boundaries be at z = 0 and z = d, and employing the boundary conditions yields the following equations,

$$1 + R = A + B \tag{4.7}$$

$$1 - R = Z(A - B) \tag{4.8}$$

$$Ae^{ink_0 d} + Re^{-ink_o d} = Te^{ik_0 d} \tag{4.9}$$

$$Ae^{ink_0 d} - Re^{-ink_o d} = \frac{1}{Z}Te^{ik_0 d} \tag{4.10}$$

Where the normalized impedance is defined as,

$$\frac{Z_1}{Z_o} = \sqrt{\frac{\varepsilon_o \mu_1}{\varepsilon_1 \mu_o}} \tag{4.11}$$

And the index of refraction of the slab is defined as,

$$n = \sqrt{\frac{\varepsilon_1 \mu_1}{\varepsilon_o \mu_o}} \tag{4.12}$$

Elimination of the A and B coefficients leads to the following equations for R and T,

$$2R = [\frac{1}{2}(1 - Z)\left(1 + \frac{1}{Z}\right)e^{ink_0 d} + \frac{1}{2}(1 - Z)\left(1 - \frac{1}{Z}\right)e^{-ink_0 d}]\,Te^{ik_0 d}$$

$$2 = [\frac{1}{2}(1 + Z)\left(1 + \frac{1}{Z}\right)e^{ink_0 d} + \frac{1}{2}(1 - Z)\left(1 - \frac{1}{Z}\right)e^{-ink_0 d}]\,Te^{ik_0 d}$$

Finally, solving for *R* and *I* yields the following

$$\frac{1}{S_{21}} = [\cos(nk_0d) - \frac{i}{2}\left(Z + \frac{1}{Z}\right)\sin(nk_0d)] \tag{4.13}$$

$$\frac{S_{11}}{S_{21}} = -\frac{i}{2}\left(Z - \frac{1}{Z}\right)\sin(nk_0d) \tag{4.14}$$

where the S-parameters are defined in terms of reflection (R) and transmission coefficients (T) as,

$$S_{11} = R$$

$$S_{21} = Te^{ik_0d}$$

In the retrieval process employed in this section, the material parameters of the medium are obtained in terms of S_{11} and S_{21} as follows,

$$Z = \pm\sqrt{\frac{(1+S_{11})^2 - S_{21}^2}{(1-S_{11})^2 - S_{21}^2}} \tag{4.15}$$

$$\text{Im(n)} = \pm Im\left(\frac{cos^{-1}\{\frac{1}{2S_{21}}[1-(S_{11}^2 - S_{21}^2)]\}}{k_0d}\right) \tag{4.16}$$

$$\text{Re(n)} = \pm Re\left(\frac{cos^{-1}\{\frac{1}{2S_{21}}[1-(S_{11}^2 - S_{21}^2)]\}}{k_0d}\right) + \frac{2\pi m}{k_0d} \tag{4.17}$$

Where, m is an unknown integer corresponding to the number of cycles a wave goes through in the slab. Note that in the above formulation it was assumed that the S-parameters are defined based on an incident wave that has a positively propagating wavefront.

Once the impedance and index of refraction have been retrieved, the relative permittivity and permeability of the slab can be directly calculated by

$$\varepsilon_r = {}^{n}/_{Z} \tag{4.18}$$

$$\mu_r = nZ \tag{4.19}$$

From the S-parameters, impedance, refractive index, effective permeability and permittivity are easily calculated and plotted using MATLAB.

Chapter 5

Results and Discussion

From numerical simulations, one can systematically study the resonant properties of high refractive index dielectric nanoparticles. To begin with, a silicon cylinder ($\varepsilon_c = 12.25, \mu_c = 1$) with radius($r = 230$ nm) is considered, where $\varepsilon_c \; and \; \mu_c$ are the relative permittivity and permeability of the silicon cylinder respectively. Height of the cylinder depends on the aspect ratio which is varied from 0.2 to 5. In this simulation, the wave propagation is along x-axis and electric field is polarized along y-axis.

5.1 Scattering Cross section

COMSOL Multiphysics, which uses finite element method simulations, is used to calculate the normalized scattering cross section (scattering cross section normalized to geometrical cross section). Using scattered field analysis in COMSOL, total scattered field source is generated. Perfect Matching Layers (PMLs) are used to prevent any unphysical scattering from the simulation boundaries. The scattering cross section for different aspect ratio of the cylinders is plotted in figure 5.1. From the plots it is observed that the resonant structures have large scattering cross section. The peaks in the normalized scattering cross section curve denote the resonance points, either electric or magnetic resonance mode. Identification of these modes is done by studying the field profiles and by the relative permeability and permittivity calculations.

Two significant peaks is observed in the plots of scattering cross section with different aspect ratio. These two peaks are mainly due to magnetic dipole and electric dipole contributions. Other small peaks are due to the magnetic and electric quadrupoles and higher order modes. In terms of Mie coefficients, first two significant peaks are due to a_1 and b_1. A clear red shift and increase in the scattering cross section as the height of the cylinder increases can be observed. Red shift means shifting of the resonance points towards longer wavelengths. The strong increase in normalized scattering cross section for larger height is due to the fact that the volume of the nanoparticle increases and thus the scattering cross section, but the geometrical scattering cross section does not change.

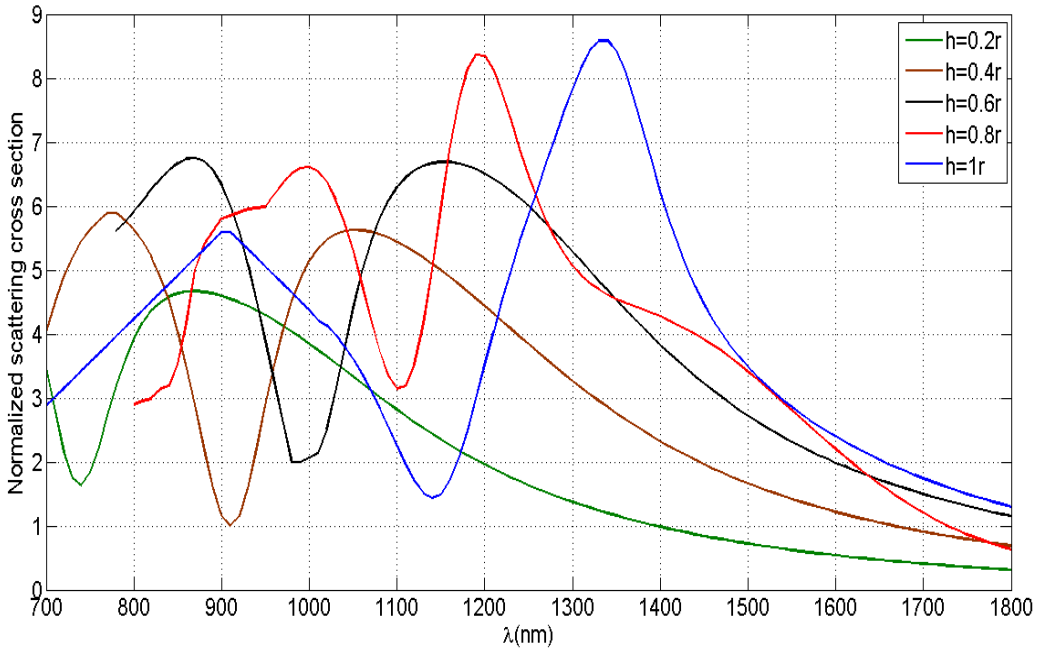

Fig. 5.1(a) Normalized scattering cross section for Si cylinder with different aspect ratio $(h = 0.2r, 0.4r, 0.6r \;\&\; 1\,r)$

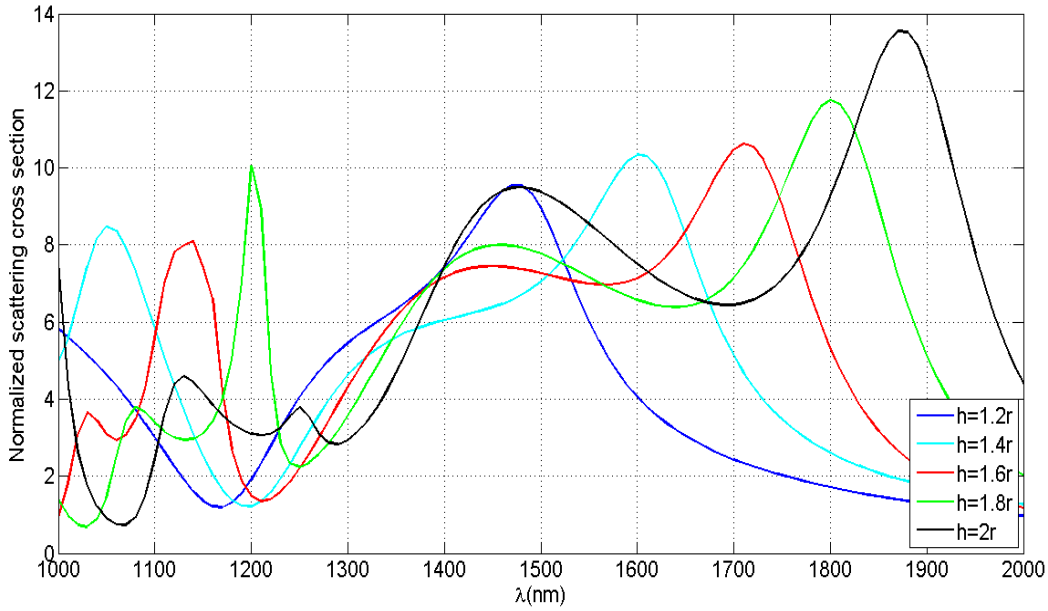

Fig. 5.1(b) Normalized scattering cross section for Si cylinder with different aspect ratio $(h = 1.2r,\ 1.4r,\ 1.6r,\ 1.8\,r \;\&\; 2r)$

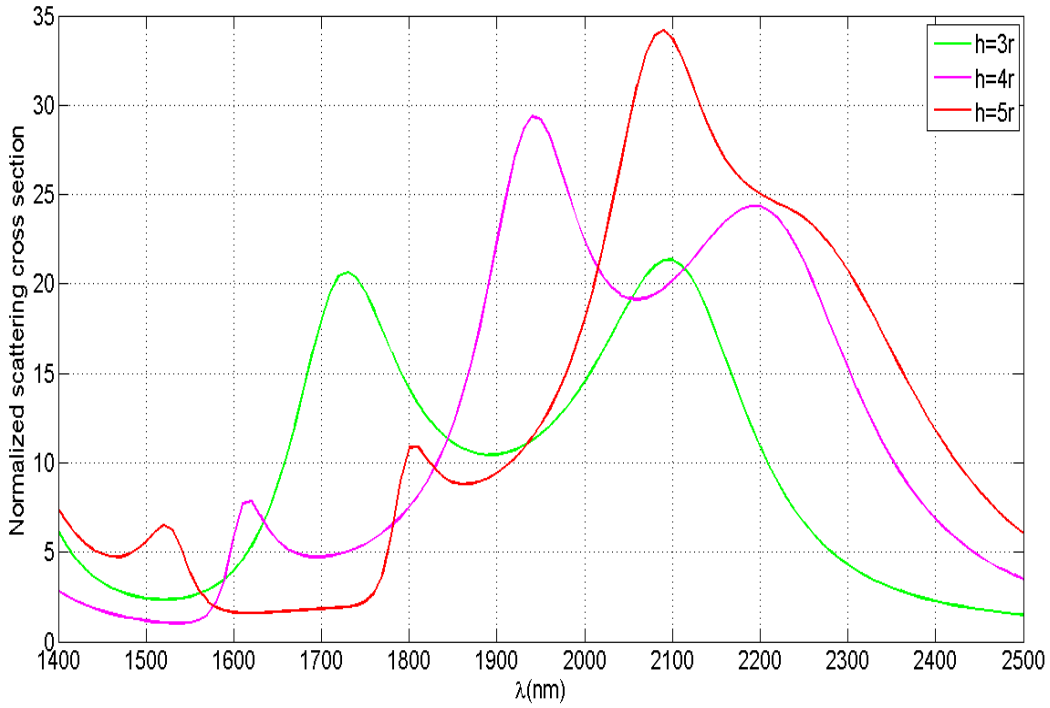

Fig. 5.1(c) Normalized scattering cross section for Si cylinder with different aspect ratio $(h = 2r, 3r \ \& \ 5\ r)$

Scattering cross section for different aspect ratio has been plotted in fig. 5.1 (a), (b) and (c). The shifting of resonance peaks towards longer wavelengths is clearly observed. As the cylinder height is increased, the peak value of scattering cross section increases as discussed earlier. There is an increasing number of higher order modes as the height increases.

5.2 Resonance modes

Mie resonances are supported by high index dielectrics is a well proven fact. Unlike plasmonic particles, the working of resonances is quite different. They are driven by displacement currents and not by actual currents. Hence these resonances are characterized by very low losses. The fundamental resonance mode is due to magnetic or electric dipole. The magnetic dipole is driven by the electric field which couples to the displacement current loops. The displacement current loop induces a magnetic dipole moment oriented perpendicular to the electric field of polarization. To drive the displacement current efficiently requires a significant retardation of the driving field throughout the particle, as the

electric field must undergo a significant phase shift in order to match the opposing electric field orientation in the top and bottom part of the particle. On the other hand, the excitation of an electric dipole requires collective polarization of material inside the resonator by the electric field component of the incident light. Identification of these modes can be done by studying the field profiles inside the particle. From figure 5.2 (a) and (b) we can observe the field lines for magnetic dipole mode. The simplest method is to calculate the relative permittivity and relative permeability. This method gives a clear cut picture of the resonance modes as the sudden change from positive to negative and then back to positive values indicate the point of resonance. For change in relative permittivity, it indicates electric resonance and for change in relative permeability it shows magnetic resonance.

There is a special case where the magnetic dipole and electric dipole modes spectrally overlap and one broad peak is observed. This occurs when the lower refractive index of the particle results in poor mode confinement and thus large radiative loss rates which occur at larger wavelengths with large nanoparticle volume. This can be again identified by studying the field profiles and corresponding current loops can be distinguished.

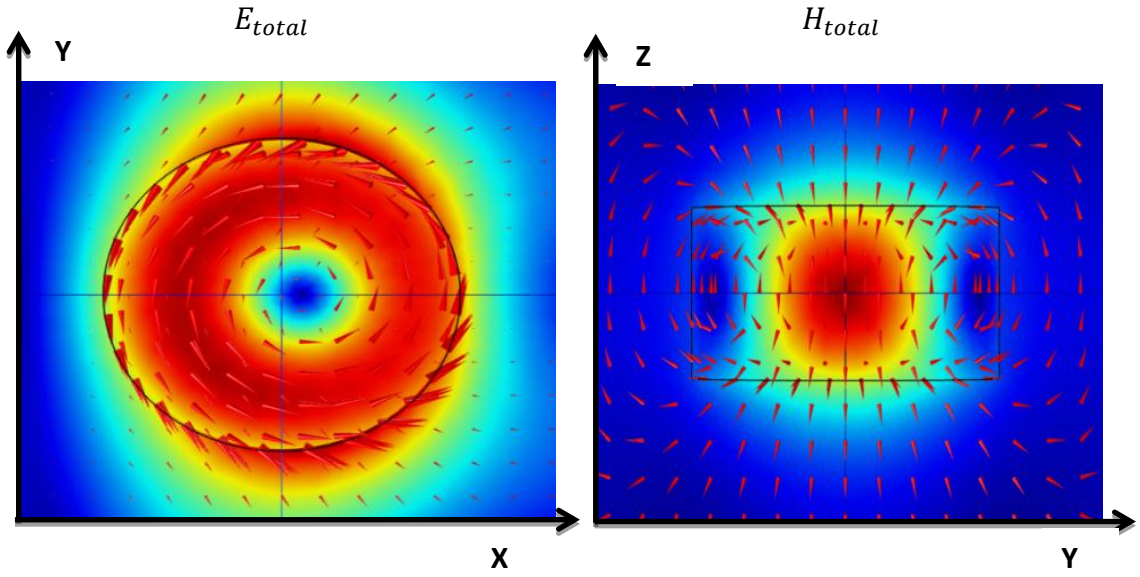

Fig 5.2: Electric (a) and magnetic (b) lines at $\lambda = 1340\ nm$ for $h = 1r$, showing resonance due to magnetic dipole.

5.3 Determination of Resonance modes.

Systematic study of the field inside the nanoparticle for determination of the mode of resonance is done. To verify, simultaneous calculation of relative permittivity, relative permeability and transmission coefficient from the s-parameters is obtained from the simulation results. These results are shown for $h = 0.2r, 1r, 2r \; and \; 5r$. The reason for its selection is to observe the changes from nano-disk to cylinder and then to nano rods. As the resonance modes is determined, it would be easy to generalize the result for cylinder with varying height.

$h = 0.2r$

The field analysis for h = 0.2r has been calculated in the range of 700-1000 nm as from the scattering cross section it is clear that the resonance point must lie in that range. As there was a single dominant peak, it would be either magnetic or electric.

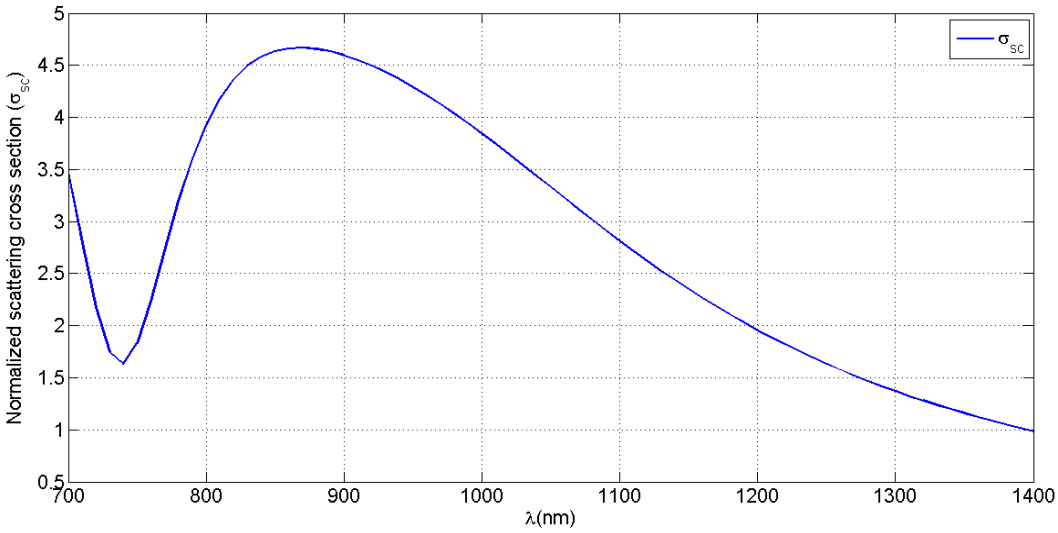

Fig. 5.3(a) : Normalized scattering cross section for $h = 0.2r$ showing only one dominant peak at λ = 870 nm.

As per Mie theory fundamental mode of a high refractive index of a sphere is always of magnetic dipole in nature. This can observed from the plots of transmission coefficient and relative permeability. There is a sharp negative peak in the plot of transmission coefficient in figure 5.3(c) at $\lambda = 867 \; nm$. This was supported by the plot of relative permeability from figure 5.3(b). Relative permittivity was observed to be constant in our desired range. This

results proves that there is magnetic dipole mode at λ = 865 nm which is observed in the field analysis. Magnetic mode is followed by electric mode but it is not observed in our desired range. Transmission coefficient calculation suggest that electric dipole mode would be found at λ = 560 nm.

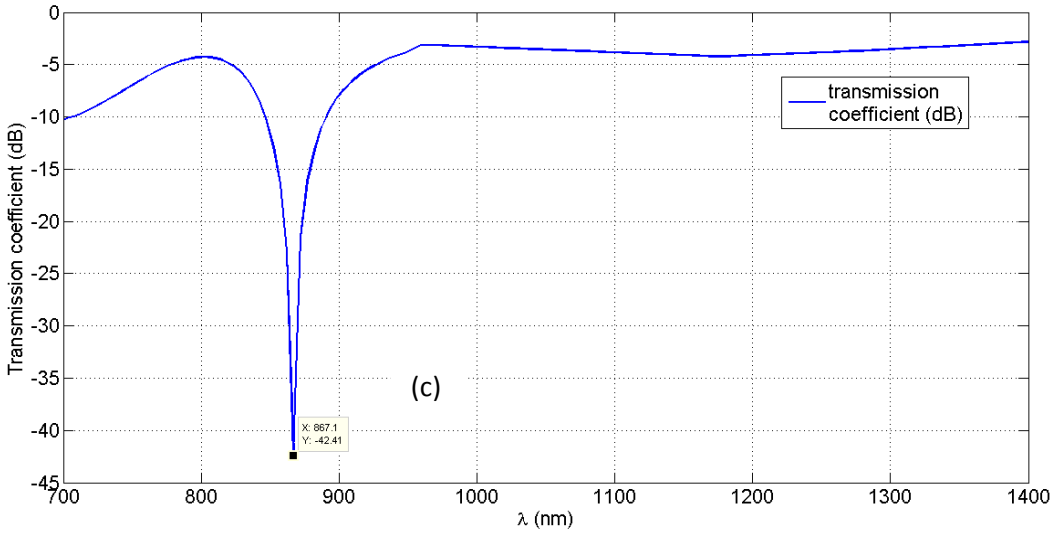

Fig. 5.3(b): Transmission coefficient for $h = 0.2r$ showing only one sharp dip at λ = 867 nm

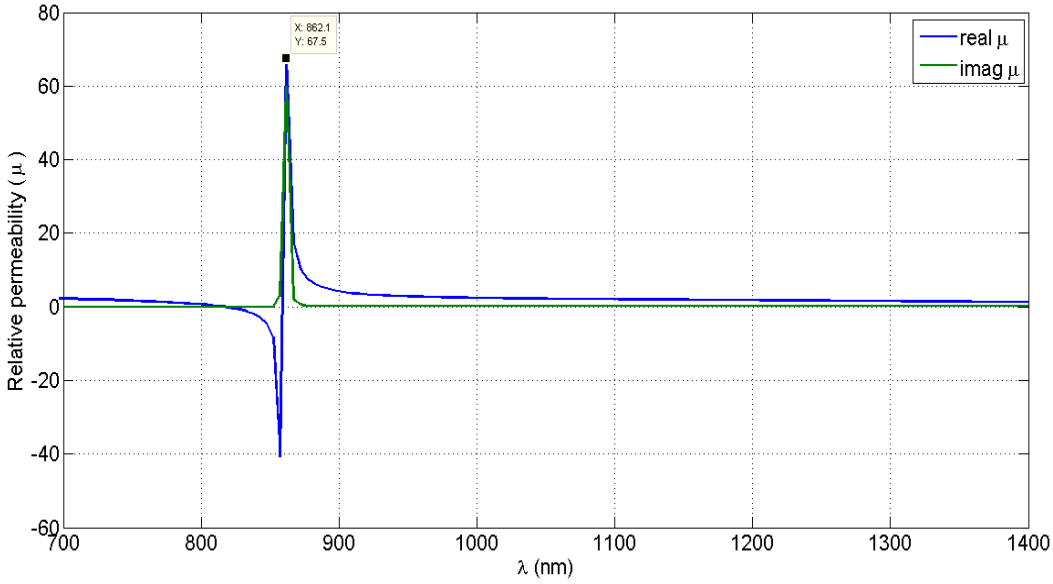

Fig. 5.3(c) : Relative permeability (μ) for $h = 0.2r$ showing only one cross over point at λ = 862 nm

$\boldsymbol{h = 1r}$

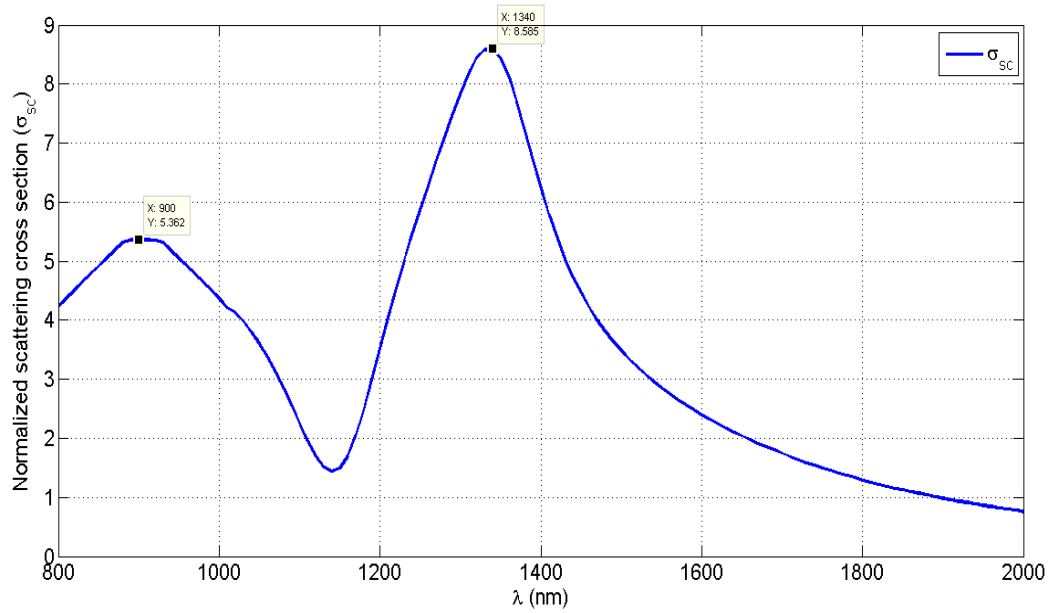

Fig. 5.4(a): Normalized scattering cross section for $h = 1r$ showing only two dominant peaks at λ = 1340 nm and 900 nm.

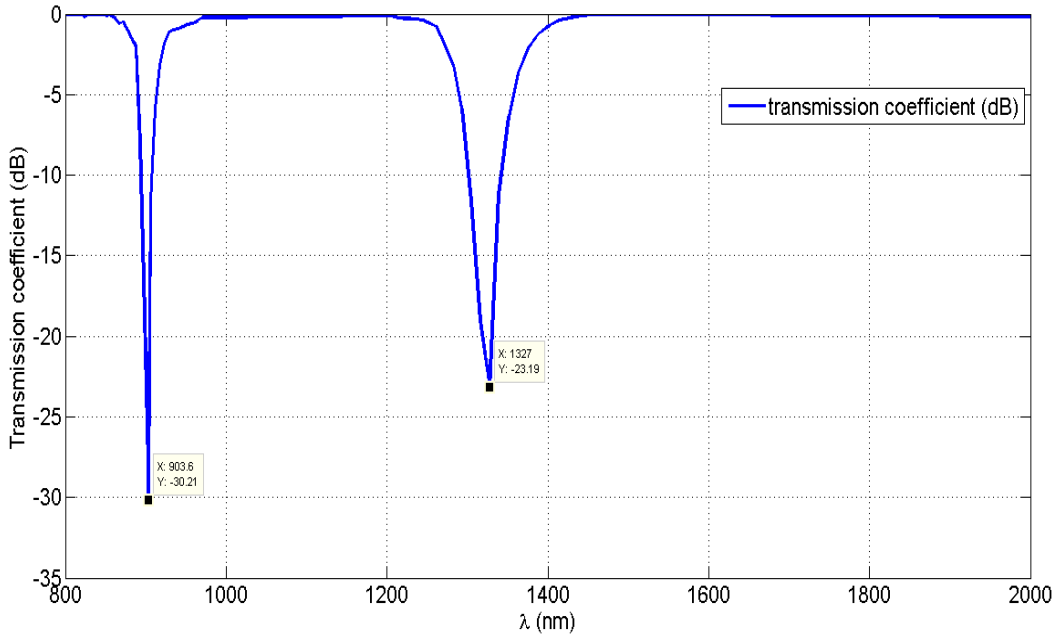

Fig. 5.4(b): Transmission coefficient for $h = 1r$ showing two sharp dips at λ = 1327 nm and 903 nm.

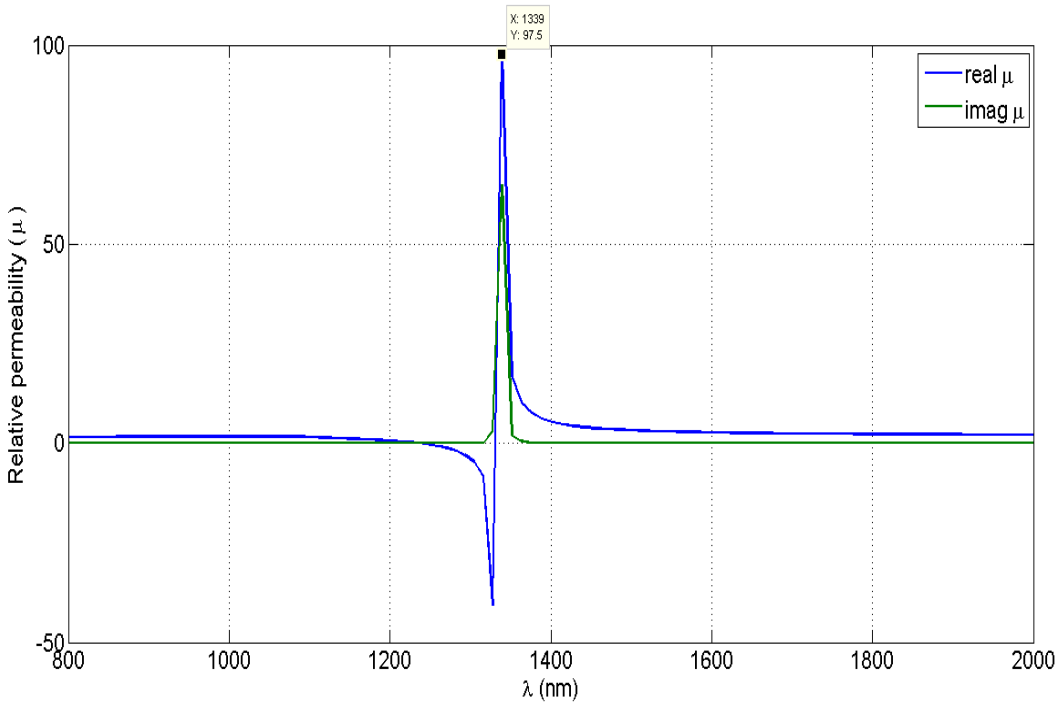

Fig. 5.4(c) : Relative permeability (μ) for $h = 1r$ showing only one cross over point at λ = 1339 nm

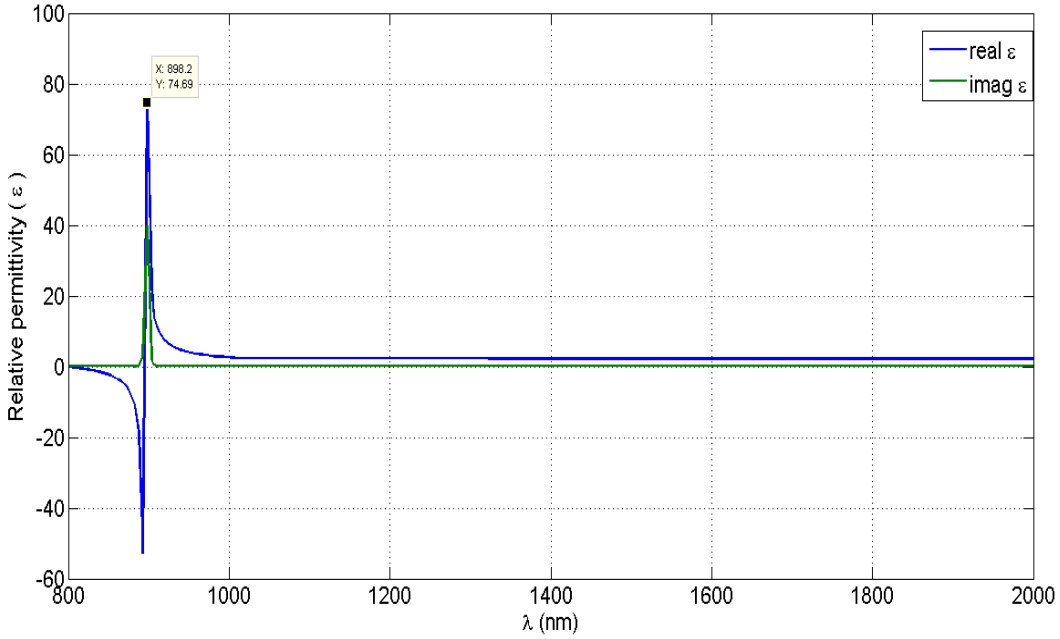

Fig. 5.4(d): Relative permittivity (ε) for $h = 1r$ showing one cross over point at λ = 898 nm

Figure 5.4(a) suggests two resonance peak points at λ = 1340 nm and λ = 900 nm. These two points are due to Mie coefficients a_1 & b_1, but to clarify the exact dominance we use transmission coefficient plots and relative permeability and permittivity plots. From fig. 5.4(b) two sharp dips are observed at 1327 nm and 903 nm. These two corresponds to the resonance points with dipole moments. A magnetic dipole is observed at λ = 1339 nm from fig. 5.4(c) and a well-supported electric dipole at λ = 898 nm. The above mentioned results are well supported with the fact that with smaller volume the hierarchy of magnetic dipole followed by electric dipole is maintained.

$\boldsymbol{h = 2r}$

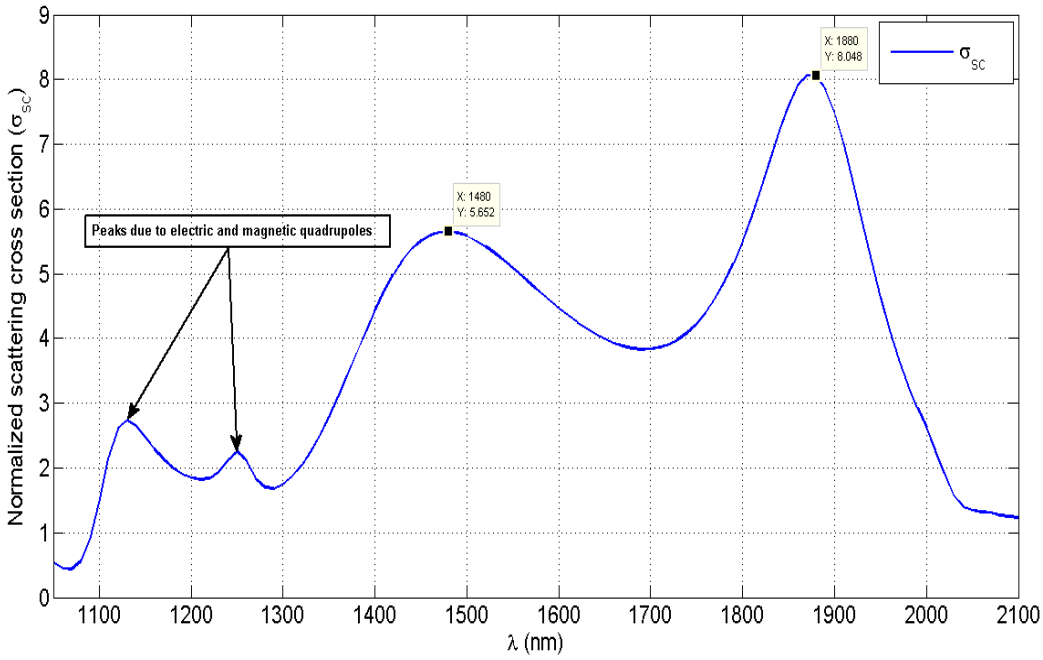

Fig. 5.5(a): Normalized scattering cross section for $h = 2r$ showing two dominant peaks at λ = 1880 nm and 1480 nm and two small peaks.

As we increase the volume of the nanoparticle the magnitude of the scattering cross section increases. This can be observed from fig. 5.5(a). The red shift in resonance peaks is clearly observed. There is a special feature that the hierarchy of magnetic followed by electric dipole is reversed in this case. It is proved with the plots of transmission coefficient (fig. 5.5(b)) and

with the calculated relative permeability and permittivity in fig. 5.5(c) and fig. 5.5(d) respectively. This change was observed prior when the aspect ratio was 1.2.

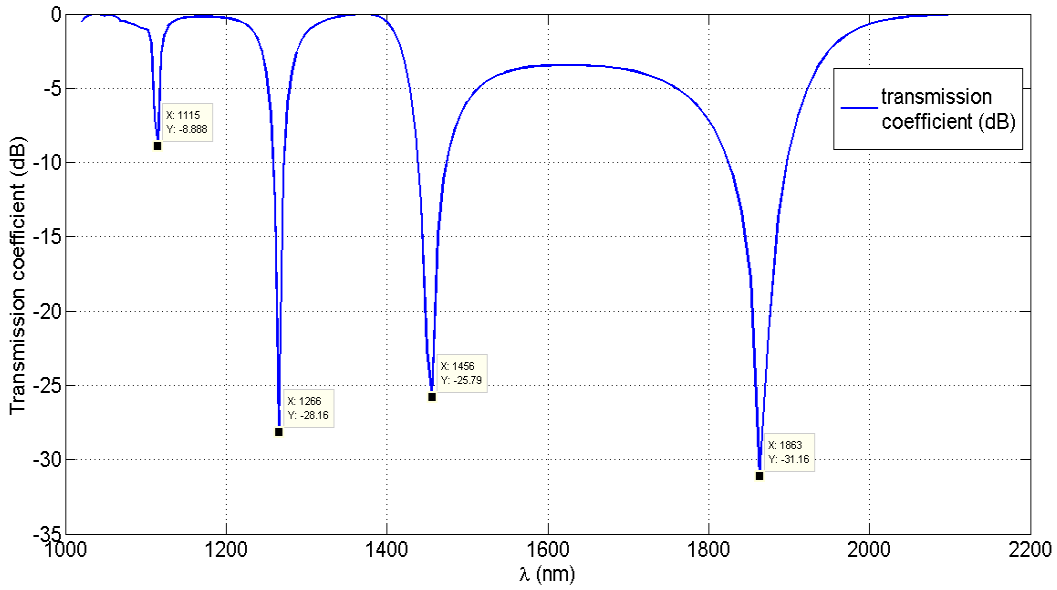

Fig. 5.5(b): Transmission coefficient for $h = 2r$ showing four sharp dips at λ = 1863 nm, 1456 nm, 1266 nm and 1115 nm.

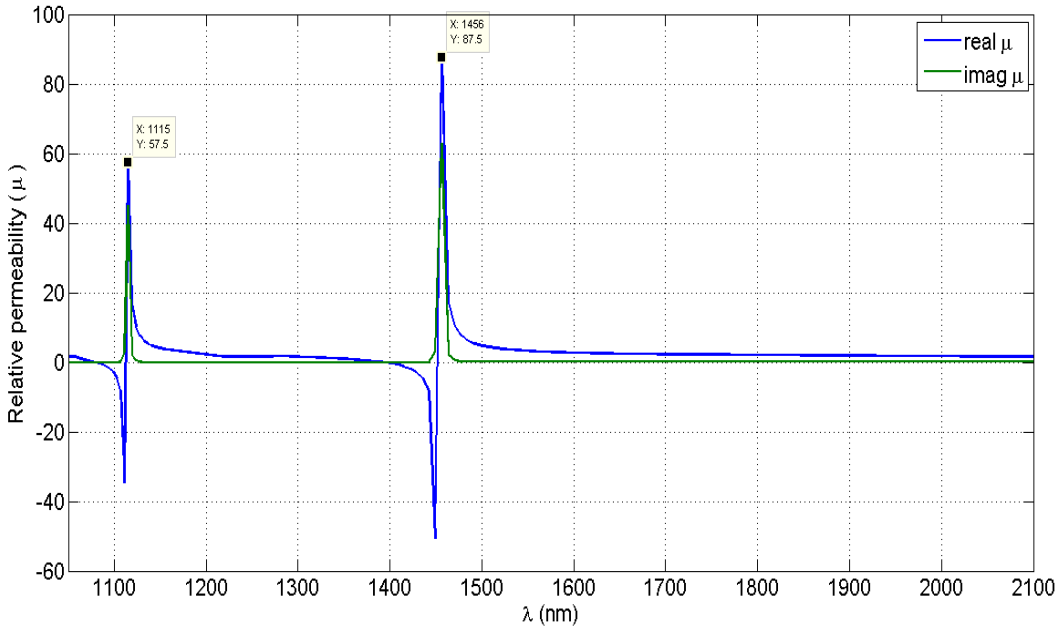

Fig. 5.5(c) : Relative permeability (μ) for $h = 2r$ showing only one cross over point at λ = 1456 nm and 1115 nm.

After the contributions of electric and magnetic dipole, we can observe small insignificant peaks which are the contributions from electric and magnetic quadrupoles. The second cross over points at lower wavelengths in fig. 5.5(c) and fig. 5.5(d) clearly indicates the presence of magnetic quadrupole and electric quadrupole respectively.

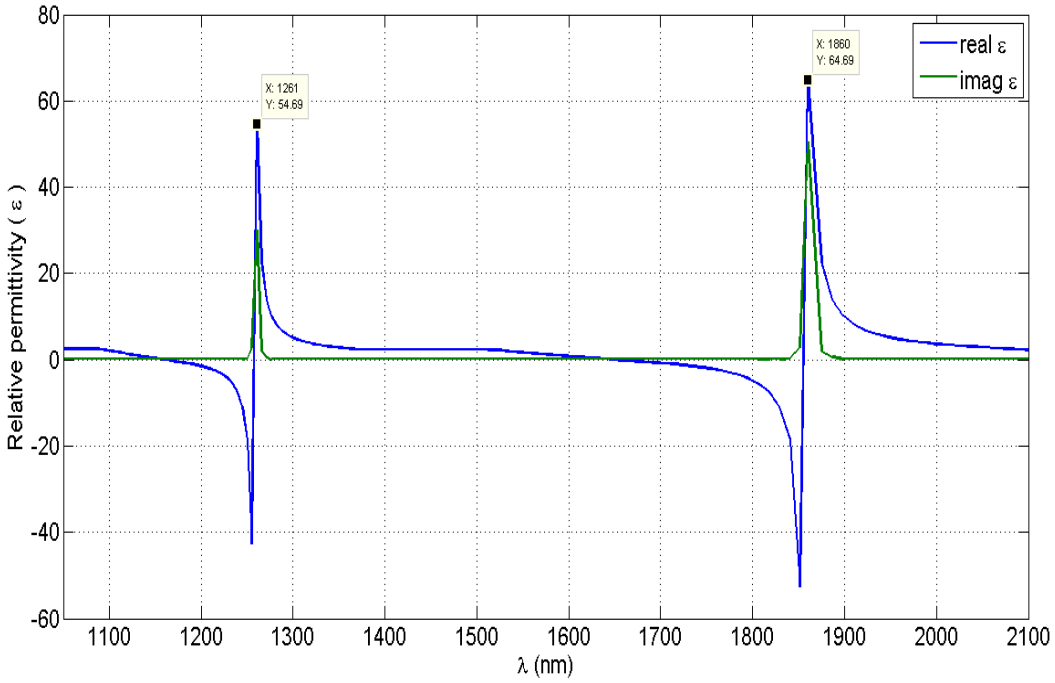

Fig. 5.5(d): Relative permittivity (ε) for $h = 2r$ showing one cross over point at λ = 1860 nm and 1261 nm.

$h = 5r$

This is an interesting case in our analysis as observed in the figure 5.6. There a single dominant peak. Transmission coefficient plot in figure 5.7 is also showing multiple dips. To find out the exact reason, electric field and magnetic field lines are studied which shows that both electric and magnetic dipole contributions. Several insignificant peaks could be found in the scattering cross section plot. These are due to higher order modes.

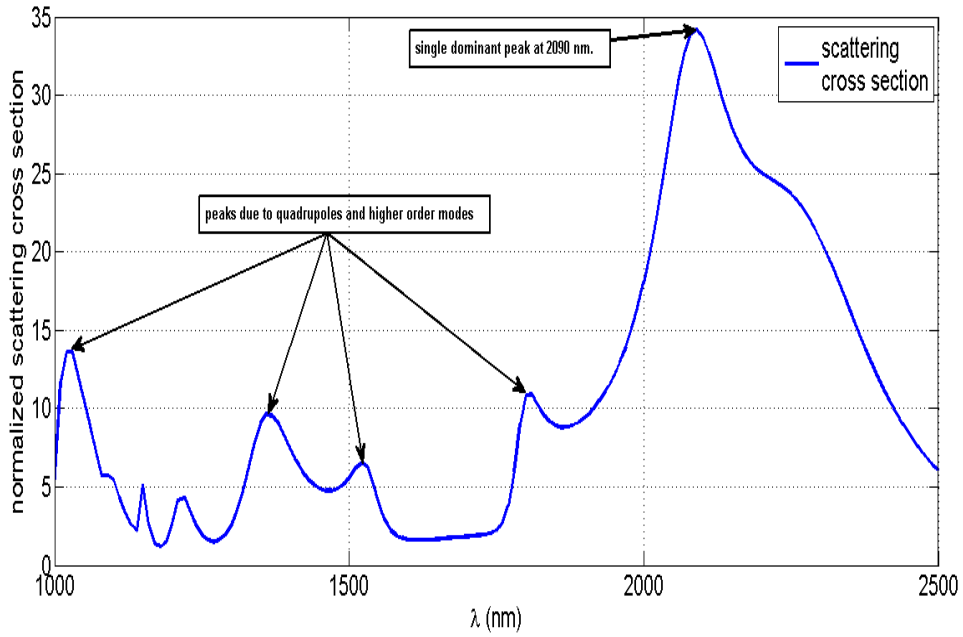

Fig 5.6: Normalized scattering cross section for cylinder (h=5r) showing single dominant peak followed by multiple small peaks.

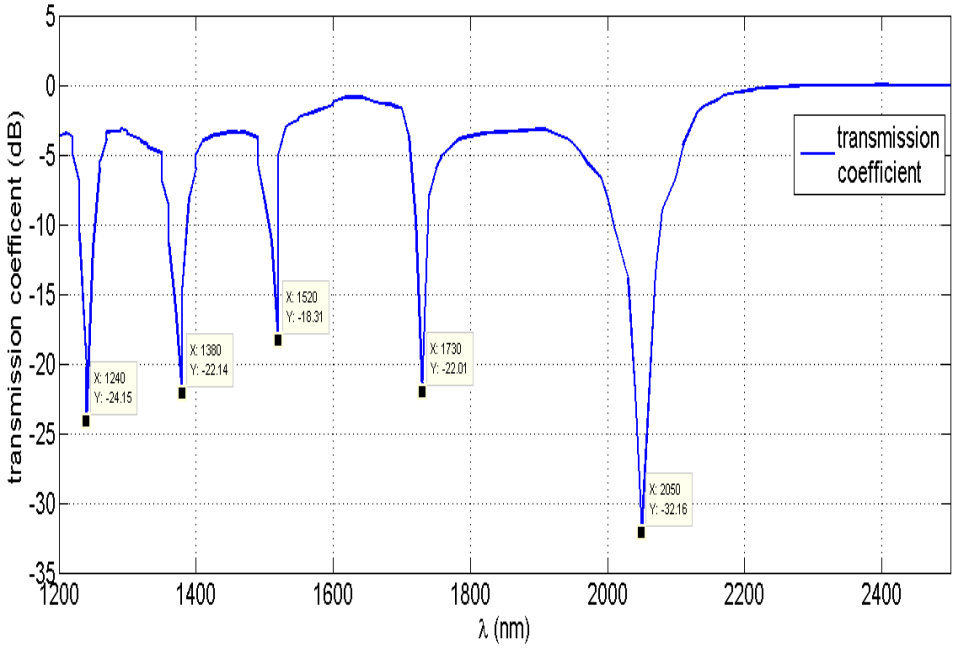

Fig 5.7: Transmission coefficient (dB) for cylinder (h=5r) showing multiple points of resonance. Resonance due to combined effect of magnetic and electric dipole is at $\lambda = 2060$ nm while other points show resonance due to higher order modes.

Chapter 6

Conclusion and scope for future work

6.1 Conclusion

In conclusion systematic study of the influence of the particle geometry on the resonant behavior of single dielectric cylindrical particles in isolated environment is done. Scattering cross section and transmission coefficient for different aspect ratio has been plotted. Using parametric retrieval technique relative permittivity and permeability are calculated which points out the type of resonance, either magnetic or electric. It is found that the lowest energy mode is an in-plane magnetic dipole mode which is driven by vertical displacement current loop inside the particle. The observed mode sequence magnetic dipole-electric dipole-magnetic quadrupole for heights less than 1.2 times radius is in accordance to the well-established mode hierarchy of magnetic and electric modes in spheres. However this hierarchy changes as we go on increasing the cylinder height. At larger heights($h > 4r$), the electric dipole and magnetic dipole spectrally overlap and the higher order magnetic quadrupole and electric quadrupole mode appears in the lower spectral range.

This work can be used as a guide line for the engineering of dielectric resonators, which facilitates to use the combined scattering from electric dipole and magnetic dipole modes to use the scattering properties for specific applications.

6.2 Scope for future work

This work can be further extended to scattering on a substrate. The effect of changing diameter can be simultaneously studied with other dielectrics. Interesting features could be found for higher refractive index. Again, the procedure for calculating relative permittivity could be used to calculate permeability within COMSOL. We have rough idea of the location of resonance points with cylinder with varying height. This method could be used to locate the resonance points for any arbitrary shape nanoparticle. A more generalized approach for arbitrary shaped nanoparticle could be established with the help of this work. This work which considers only a single nanoparticle, could be for the multi arrayed nanoparticles.

References

1. L. Novotny and B. Hecht, Principles of Nano-Optics (Cambridge University Press, 2012).
2. C. M. Soukoulis and M. Wegener, "Past achievements and future challenges in the development of three-dimensional photonic metamaterials," Nat. Photonics 5, 523–530 (2011).
3. L. Novotny and N. Van Hulst, "Antennas for light," Nat. Photonics 5, 83–90 (2011).
4. Alu and N. Engheta, "Tuning the scattering response of optical nanoantennas with nanocircuit loads," Nat. Photonics 2, 307–310 (2008).
5. W. Xiong, D. Sikdar, M. Walsh, K. J. Si, Y. Tang, Y. Chen, R. Mazid, M. Weyland, I. D. Rukhlenko, J. Etheridge et al., "Single-crystal caged gold nanorods with tunable broadband plasmon resonances," Chem. Commun. 49, 9630–9632 (2013).
6. H. A. Atwater and A. Polman, "Plasmonics for improved photovoltaic devices," Nat. Mater. 9, 205–213 (2010).
7. D. Sikdar, I. D. Rukhlenko, W. Cheng, and M. Premaratne, "Optimized gold nanoshell ensembles for biomedical applications," Nanoscale Res. Lett. 8, 142–146 (2013).
8. S. Lal, S. Link, and N. J. Halas, "Nano-optics from sensing to waveguiding," Nat. Photonics 1, 641–648 (2007).
9. U. Kreibig and M. Vollmer, Optical Properties of Metal Clusters (Springer-Verlag, Berlin, 1995).
10. D. R. Smith, J. B. Pendry, and M. C. K. Wiltshire, Science 305, 788 (2004).
11. J. B. Pendry, Nature Mater. 5, 763 (2006).
12. D. Schurig et al., Science 314, 977 (2006).
13. K. C. Huang, M. L. Povinelli, and J. D. Joannopoulos, Appl. Phys. Lett. 85, 543 (2004).
14. M. S. Wheeler, J. S. Aitchison, and M. Mojahedi, Phys. Rev. B 72, 193103 (2005).
15. L. Jyhl¨a et al., J. Appl. Phys. 99, 043102 (2006).
16. L. Peng et al., Phys. Rev. Lett. 98, 157403 (2007).
17. J. A. Schuller et al., Phys. Rev. Lett. 99, 107401 (2007).
18. C. M. Soukoulis et al., Phys. Stat. Sol. B 244, 1181 (2007).

19. H. C. van de Hulst, Light Scattering by Small Particles (Dover Publications, Inc., NY, 1981).

20. R. K. Mongia, and P. Bhartia, "Dielectric resonator antennas-A review and general design relations for resonant frequency and bandwidth," Int. J. Microwave Millimeter-Wave Comput.-Aided Eng. 4, 230247 (1994).

21. . R. C. J. Hsu, A. Ayazi, B. Houshmand, and B. Jalali, "All-dielectric photonic-assisted radio front-end technology," Nat. Photonics 1, 535538 (2007).

22. Jon A. Schuller and Mark L. Brongersma, "General properties of dielectric optical antennas," Opt. Express 17, 24084-24095 (2009).

23. C. F. Bohren and D. R. Huffman, Absorption and Scattering of Light by Small Particles (JohnWiley &Sons, New York, 1998).

24. M. I. Mishchenko, L. D. Travis and A. A. Lacis, Scattering, Absorption, and Emission of Light by Small Particles (Cambridge Univ. Press, 2002).

25. Staude, I. et al. Tailoring directional scattering through magnetic and electric resonances in subwavelength silicon nanodisks. ACS Nano 7, 7824–7832 (2013).

26. Vynck, K., *et al.,* "All-dielectric rod-type metamaterials operating at optical frequencies," http://arxiv.org/abs/0805.0251 (2008).

27. Zhao, Q., Zhou, J., Zhang, F. & Lippens, D. Mie resonance-based dielectric metamaterials. *Mater. Today* **12,** 60–69 (December, 2009).

28. D. R. Smith, D. C. Vier, Th. Koschny and C. M. Soukoulis, Electromagnetic parameter retrieval from inhomogeneous metamaterials, PHYSICAL REVIEW E **71**, 036617 (2005)